Developing ocean particle tracking tools for cross-disciplinary oceanic research with applications in the Agulhas Current region

Michael G. Hart-Davis

Submitted in fulfilment of the requirements for the degree of

Master of Science (Physical Oceanography)

in the Faculty of Science

at the Nelson Mandela University

Date of Submission - 1st August 2019

Supervisors:

Associate Prof Mostafa Bakhoday-Paskyabi, Dr Björn C. Backeberg,

Prof Juliet C. Hermes and Prof Johnny A. Johannessen

NELSON MANDELA UNIVERSITY

DECLARATION BY CANDIDATE

NAME: Michael Geofrey Hart-Davis

STUDENT NUMBER: s218197187

QUALIFICATION: Master of Science: Physical Oceanography

TITLE OF PROJECT: Developing ocean particle tracking tools for cross-disciplinary oceanic research with applications in the Agulhas Current region

DECLARATION:

In accordance with Rule G5.6.3, I hereby declare that the above-mentioned treatise/ dissertation/ thesis is my own work and that it has not previously been submitted for assessment to another University or for another qualification.

SIGNATURE: 

DATE: 22 October 2019

Developing ocean particle tracking tools for cross-disciplinary oceanic research with applications in the Agulhas Current region

Abstract

Lagrangian ocean analysis is a powerful way to study ocean processes from in-situ observations and numerical model simulations. As numerical modelling capabilities develop and physical mechanisms of the ocean are better understood, the importance of particle trajectory modelling continues to increase. Therefore, developing cross-disciplinary particle trajectory model applications for the Greater Agulhas System is highly relevant due to its potential contribution to scientific studies and operational applications. This thesis presents the results of developing particle trajectory model applications in the Greater Agulhas System towards better understanding the physical mechanisms that drive ocean processes in the region. The model is used in three applications that demonstrate their cross-disciplinary potential. These applications include a search and rescue scenario, the study of ocean dynamics and the study of the fate of juvenile turtles. Introducing spatially and temporally varying stochastic motion to account for the processes not resolved in the ocean surface current products, as well as including more appropriate boundary conditions, were shown to improve the accuracy of virtual drifters in representing the trajectory of a real surface drifter. Next, implementing the spatially and temporally varying stochastic motion in the particle trajectory model and applying it to a search and rescue scenario of a capsized catamaran revealed that including both winds and surface ocean currents in the particle trajectory model allowed for an improved prediction of the capsized vessel's trajectory.

By comparing a pair of real surface drifters with the particle trajectory model and analysing high resolution sea surface temperature (SST) fields it was shown that the formation of an eddy on the Agulhas Plateau combined with the weakening of the core current velocity resulted in enhanced eddy-current interactions facilitating the separation of the real surface drifter-pair as they passed through this region. Lastly, the particle trajectory model was used to study the importance of including active swimming characteristic when studying the fate of juvenile turtles. It was found that including active swimming resulted in a change in the distribution of juvenile turtles and, therefore, needs to be included to provide a proper understanding of the fate of juvenile turtles in the ocean. With further development and refinement of the particle trajectory model, Lagrangian ocean analysis has the potential to provide valuable information towards improving our understanding of physical and biological ocean processes at a range of spatial and temporal scales with potential operational oceanography applications.

Declaration

I, **Michael G. Hart-Davis**, declare that this work has not been previously submitted in whole, or in part, for the award of any degree. The contribution and quotation of others works in this dissertation has been acknowledged, cited and referenced. The present work entitled "Lagrangian ocean analysis to study the physical mechanisms driving the processes occurring in the Greater Agulhas Current System" has been originally written by me, with the full support of my supervisors:

Dr Björn C. Backeberg

EGI Foundation, Amsterdam, Netherlands

Nansen Environmental and Remote Sensing Center, Norway

Prof Juliet C. Hermes

South African Earth Observation Network, Cape Town, South Africa

Nelson Mandela University, Port Elizabeth, South Africa

University of Cape Town, Cape Town, South Africa

Associate Prof Mostafa Bakhoday-Paskyabi

Geophysical Institute, University of Bergen, Bergen, Norway

Nansen Environmental Remote Sensing Center, Bergen, Norway

Prof Johnny A. Johannessen

Nansen Environmental Remote Sensing Center, Bergen, Norway

Publication based on the present work:

Hart-Davis, M.G., Backeberg, B.C. and Bakhoday-Paskyabi, M. 2018b. An assessment of the importance of combining wind, ocean currents and stochastic motions in a particle trajectory model for search and rescue applications. SASAS: Interactions between the atmosphere and ocean. Available: http://sasas.ukzn.ac.za/

Acknowledgements

This work is based on the research supported in part by the National Research Foundation of South Africa (Grant Numbers: 112105), the Nansen-Tutu Centre at the University of Cape Town and the Egagasini Node of the South African Earth Observations Network (SAEON).

I would like to further thank the NRF, Nansen-Tutu Centre and SAEON for allowing me to travel to Bergen, Norway and Utrecht, Netherlands. Staying in Bergen for almost a year, was extremely valuable. I was able to build relationships with scientists, gaining knowledge and improving the overall quality of my thesis.

Thank you to my supervisors; Dr Björn Backeberg, Prof Juliet Hermes, Associate Prof Mostafa Bakhoday-Paskyabi and Prof Johnny Johannessen; for their support and integral input towards completing this thesis. All have contributed a lot of time (patience) and knowledge in explaining concepts and discussing the thesis, for which I am very grateful! The opportunities and experience that I have gained from all of you will never be forgotten.

I would like to thank all the scientists and admin staff at the Nansen Environmental Remote Sensing Center in Bergen, Norway for allowing me to visit and learn from world-renowned experts in the field of oceanography. The experience that I had and the people I was fortunate enough to meet, will remain with me for the rest of my career.

I would like to thank scientists and lecturers at the University of Bergen particularly Prof Knut Barthel and Dr Knut-Frode Dagestad. The classes I was able to attend and the conversations we had about numerical modelling and particle trajectory modelling have helped shape my understanding of concepts and processes.

Thank you to Associate Prof Erik van Sebille, who helped with understanding OceanParcels and gave valuable comments and input throughout my entire thesis.

To everyone who is part of the OceanParcels team at the University of Utrecht, thanks for hosting me and making me feel part of the family. I appreciate the relationships that I have built during my stay!

Lastly, I would like to thank my family and friends for their support and patience throughout my extended absence from home.

Michael Geoffrey Hart-Davis

Cape Town, South Africa

August 2019

Contents

Listing of figures

1

Introduction

Particle trajectory modelling is a novel technique with applications in several important ocean disciplines - fish egg and larval dispersal (Thorpe et al., 2004, Singh et al., 2018), spreading and concentration of litter (Onink, 2018) and oil spill modelling (Sayol et al., 2014). With the advancement of computing capabilities, numerical models have been able to run at higher spatial and temporal resolutions resulting in an increased number of applications for particle trajectory modelling. Different techniques and tools have been developed using particle trajectory modelling that have been applied to different scientific applications.

Although the tools follow the same general equations, they mainly differ in the interpretation techniques used in the calculation of the particle trajectories and their parameterization. One of these parameters, stochastic motion, is important in simulating diffusion, accounting for physical processes (Van Sebille et al., 2018) that are not resolved by the numerical models due to limitations in the spatial and temporal resolution. In most studies, accounting for these sub-grid scale processes is important in providing trajectories that have a more accurate representation of reality.

The calculation of stochastic motion is complex in terms of formulation and methodology. Moreover, boundary conditions become more important with the inclusion of stochastic motion. Boundaries occur at the edge of the numerical model domain and land-sea borders. The virtual particles' interaction with the boundary may require a particular boundary condition to be set dependent on the process being studied.

Several studies have been conducted in the greater Agulhas Current utilizing particle trajectory modelling. For example: in validating ocean products (Hart-Davis et al., 2018b); studying ocean dynamics (van Sebille et al., 2009, Ragoasha et al., 2019); marine larval dispersion (Singh et al., 2018); plastic dispersion (Collins and Hermes, 2019); and search and rescue (Hart-Davis et al., 2018a). More recently, improvement of numerical models in the representation of physical processes in the Agulhas Current (Backeberg et al., 2014, Veitch and Penven, 2017, Schwarzkopf et al., 2019) have opened the door for a greater amount of processes to be studied in the region.

A variety of dynamical ocean processes characterise the greater Agulhas Current system, determining its structure. The greater Agulhas Current system plays an important role in the local weather patterns of southern Africa and the global climate system (Beal et al., 2011, Nkwinkwa Njouodo et al., 2018, Imbol Nkwinkwa et al., 2019). Furthermore, the system's complex physical processes have a drastic impact on the biodiversity of the marine environment and the distribution of marine organisms around South Africa. The current also influences marine shipping as it lies on the path of major shipping lanes linking Indian Ocean countries and Atlantic Ocean countries.

The meso- and sub-mesoscale variability of this region is extremely complex and still not fully understood, particularly in the Agulhas Plateau region (Backeberg et al., 2008, Le Bars et al., 2013), south of the South African coast. There are a variety of techniques used to study the dynamics of the Agulhas Current system, including the use of virtual particle tracking (Doglioli et al., 2006, Blanke et al., 2009, Durgadoo et al., 2013, Cheng et al., 2016, Veitch et al., 2018, Ragoasha et al., 2019). The research done in these studies suggests that virtual particle tracking can be used to study the pathways of the Agulhas Current system as represented in numerical models.

The hypothesis that will be tested during this thesis is that: *Lagrangian ocean analysis can be used to provide a better understanding of the physical mechanisms that drive the processes occurring in the Greater Agulhas System*. The specific objectives are:

- To develop the appropriate Lagrangian parameterizations to optimize the particle trajectory model for use in different experiments.
- To assess the accuracy of a particle trajectory model that combines surface currents, windage and stochastic motion in search and rescue applications.
- To use the developed particle trajectory model to study the sub-mesoscale variability of the Agulhas Plateau using the trajectory of two surface drifters.
- To evaluate the importance of including the initial swim speed of juvenile loggerhead turtles when modelling their drift in the Greater Agulhas System.

The study is organized as follows: Chapter 2 presents a literature review that includes a general description of the Agulhas Current system; Lagrangian ocean analysis; search and rescue operations; and juvenile loggerhead turtles. Chapter 3 describes the data used in this thesis as well as a description of the methodology used to calculate Lagrangian eddy diffusivity. The results presented in Chapter 4 are divided into four subsections.

Subsection 4.1 presents the results of the developed parameters of Lagrangian ocean analysis that will be used in the sections that follow as well as application in a search and rescue. Subsection 4.2 focuses on assessing the trajectory of two drifters using two surface ocean products to understand the mesoscale variability of the Agulhas Plateau. A study showing the importance of including the initial swim speeds when modelling the trajectory of juvenile loggerhead turtles is presented in Subsection 4.3. The most significant findings and conclusions of this study are summarized in Chapter 5.

2

Literature Review

Western boundary currents (WBCs) - such as the Gulf Stream in the North Atlantic, Kuroshio in the North Pacific, the East Australian Current in the South Pacific and the Agulhas Current in the South Indian Ocean - are strong, persistent currents that transport subtropical waters along the western boundaries of the world's major ocean basins towards the poles (Seager and Simpson, 2016). They transport significant amounts of heat, impact shelf and coastal regions and are regions of intense air/sea fluxes (Atkinson, 2010).

Therefore, understanding how these current systems work is fundamental to understanding the earth's global climate engine. Typically, WBCs have widths of approximately 100 km and average speeds of 1 $m.s^{-1}$, with the strength of the current decreasing with depth (Imawaki et al., 2013). WBCs are regions of strong air-sea interaction thus playing an important role in the local weather patterns and global climate. The warm water being transported by these currents is cooled and evaporated by cold, dry continental air masses which are carried over the WBCs by the prevalent westerly winds (Imawaki et al., 2013). WBCs absorb large amounts of atmospheric CO_2 (Takahashi et al., 2009, Imawaki et al., 2013), which is important for photosynthetic organisms that reside in the ocean.

The WBCs have several similar traits, but each current has its own unique characteristics (Lutjeharms, 2006). Driven by the zonally integrated wind-stress curl of the adjacent oceanic basins (Lutjeharms, 2006), meanders and Rossby-wave like motion is often associated with the separation of the WBC from the continental margins (da Silveira et al., 1999). As a result of the separation, the current may either continue to meander towards the ocean basin (e.g. the Gulf Stream) or the current can overshoot its separation location and retroflect (e.g. the Agulhas Current) (da Silveira et al., 1999). In both types of separation, eddy detachment may occur. These eddies, with diameters ranging between 200-250 km depending on region (Lutjeharms, 2006, Garcia-Jove et al., 2016), transport warm water masses which is important for global ocean circulation and climate variability (Kelly and Dong, 2004, Beal et al., 2011).

2.1 Agulhas Current System

The Agulhas Current is one of the fastest flowing WBCs in the world, with mean maximum velocities of about 1.5 $m.s^{-1}$, and often exceeding 2 $m.s^{-1}$ (Rouault et al., 2010). The Agulhas Current System plays a key role in the local weather patterns of southern Africa as well as the global climate (Beal et al., 2011, Nkwinkwa Njouodo et al., 2018). It also plays a pivotal role in the global thermohaline circulation (Gordon, 1986) and the Meridional Overturning Circulation of the Atlantic Ocean (Biastoch et al., 2008a).

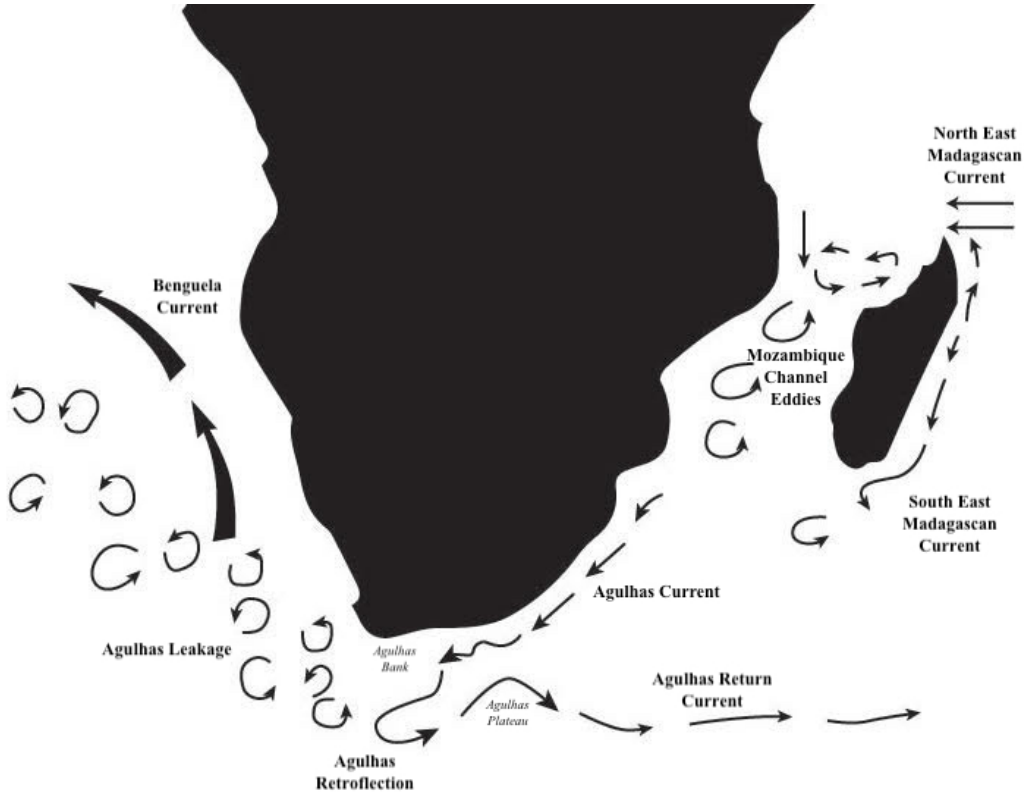

Figure 2.1: Schematic of the Agulhas Current system adapted from Lutjeharms and Ansorge (2001) illustrating all the major oceanographic features.

The system consists of several oceanic features that all play unique roles in characterising the Agulhas Current System (Figure 2.1). These features include, but are not limited to: the Agulhas Current, the Agulhas Retroflection and the Agulhas Return Current. These features are discussed below.

2.1.1 Agulhas Current

Hundreds of research papers have been published on the Agulhas Current, illustrating its importance on local and global processes. It influences the oceanography of coastal and shelf regions through a range of large scale (> 100-200 km), mesoscale (50 - 100 km) and submesoscale (<10 km) processes, such as eddy shedding, plumes, filaments and the intrusion of the current onto the coastal shelf (Lutjeharms, 2006). The Agulhas Current is divided into two different parts, the northern and southern Agulhas Current, which exhibit distinct differences in path characteristics (Lutjeharms et al., 2003) that combine to give the Agulhas Current its unique shape.

Northern Agulhas Current

The northern Agulhas Current is considered to be unusually stable for a WBC as the current is steered along a narrow, steep continental slope (Lutjeharms, 2006). Studies using acoustic current profilers (Beal and Bryden, 1997) have shown a maximum surface current speed of 1.7 $m.s^{-1}$ with the core being on average 219 km wide (Beal et al., 2015) and reaching a depth of 2,500 meters (Beal and Bryden, 1999, Lutjeharms, 2006). The relatively stable nature of the current implies that there is very little meandering taking place (Lutjeharms, 2006), with the current on average meandering less than 15 km to either side (Gründlingh, 1983). However, large solitary meandering events, commonly referred to as the Natal Pulse, are a well-documented feature of the northern Agulhas Current (Lutjeharms and Roberts, 1988). Studies have shown that these events occur on average 1.6 times a year (Rouault et al., 2010), although there have been recorded periods where up to six events have been observed (de Ruijter et al., 1999). The Natal Pulse moves downstream at an estimated speed of 19 - 20 $cm.s^{-1}$ (Lutjeharms and Roberts, 1988) and has an impact on the dynamics of the surrounding regions.

Variability in this region is influenced by both cyclonic and anticyclonic eddies, originating from the Mozambique Channel and south of Madagascar (Backeberg and Reason, 2010, Braby et al., 2016). Recent studies demonstrate seasonal variability in the geostrophic velocity of the Agulhas Current but no variation in the width of the Agulhas Current's core (Krug and Tournadre, 2012, Beal et al., 2015).

Southern Agulhas Current

As the current continues to flow southward, the topographic steering of the current begins to weaken which results in larger meanders of the current (de Ruijter et al., 1999). This is said to be a result of the current flowing over the widening Agulhas Bank which causes a more unstable regime (Lutjeharms, 2006). The mean annual surface velocities in the southern Agulhas Current range between 1.5 $m.s^{-1}$ and 2 $m.s^{-1}$, with depths of the current extending to the seafloor (Casal et al., 2009) and the mean width averaging around 100 km (Lutjeharms, 2006). Satellite altimetry has demonstrated that there is higher mesoscale variability in the sea level anomaly (SLA) when compared to the northern Agulhas Current (Wakker et al., 1990), which is thought to be a result of the increased meandering of the current (Lutjeharms, 2006).

2.1.2 Agulhas Retroflection

South of the Agulhas Bank, the Agulhas Current begins to turn eastward in an anticyclonic loop known as the Agulhas Retroflection. The loop has an average diameter of about 340 km ± 70 km (Lutjeharms, 2006), with its exact geographical position varying between 27°E and 32°E (Lutjeharms and Van Ballegooyen, 1988, Lutjeharms, 2006). The Retroflection contains some of the highest levels of mesoscale variability in the world's ocean (Garzoli et al., 1996) and is associated with the formation and shedding of large anticyclonic eddies known as Agulhas Rings (Lutjeharms and Van Ballegooyen, 1988, de Ruijter et al., 1999). These Agulhas Rings have an average diameter of 324 ± 94 km (Lutjeharms, 2006), with observations showing these rings travel between 5 to 8 km/day away from the Retroflection (Olson and Evans, 1986). These rings as well as eddies and filaments (Biastoch et al., 2008b, Beal et al., 2011) transport warm and salty water from the Indian Ocean into the South Atlantic Ocean and are the main contributors to the Agulhas leakage (Gordon, 1986). The Agulhas Leakage which represents the amount of water transferred from the Indian to the Atlantic oceans by the Agulhas Current is thought to play a crucial role in the global climate system (Beal et al., 2011).

2.1.3 Agulhas Return Current

The eastward flow resulting from the Agulhas Retroflection, the Agulhas Return Current, lies at about 40°S and extends into the South-Indian Ocean as far as 70°E (Lutjeharms, 2006). The core width of this current is around 70 km wide, with the mean velocities reaching up to 2 $m.s^{-1}$ (Lutjeharms and Ansorge, 2001, Backeberg et al., 2008). It is characterized by strong mesoscale variability as a result of eddy generation (Lutjeharms and Valentine, 1988, Lutjeharms and Ansorge, 2001) as well as large solitary meanders. These meanders are topographically induced by the irregular seafloor topography of the region (Lutjeharms, 2006). The first of these quasi-stationary meanders occurs around the Agulhas Plateau around 25°E and 29°E (Pichevin et al., 1999).

2.1.4 Agulhas Plateau

The Agulhas Plateau is located south of South Africa in the South-West Indian Ocean (Figure 2.2) and rises about 2,500 m from the surrounding deeper ocean of 4,700 m (Parsiegla et al., 2008). A cyclonic-like meander around the Agulhas Plateau can be depicted in satellite altimetry, passive microwave sea surface temperature fields and numerical model simulations (Backeberg et al., 2008, Renault et al., 2017) as well as in surface drifter observations (Lutjeharms, 2006). Large, warm anticyclonic eddies are known to occur on the Agulhas Plateau (Morris et al., 2017), with east-west diameters of up to 600 km and north-south diameters of 200 km (Lutjeharms, 2006). However, the mechanisms affecting the mesoscale variability in this region remains unclear (Backeberg et al., 2008). A study by Lutjeharms and Valentine (1988) used satellite imagery to suggest the prevalence of large warm eddies over the Agulhas Plateau. Furthermore, satellite remote sensing has shown that the area in the vicinity of the Agulhas Plateau is particularly active for cross-frontal eddy shedding (Lutjeharms and Valentine, 1988). It is expected that the mesoscale variability introduced by the eddy formed on the Agulhas Plateau could have a substantial influence of the Agulhas Return Current trajectory, therefore, it is important to develop a deeper understanding of this region.

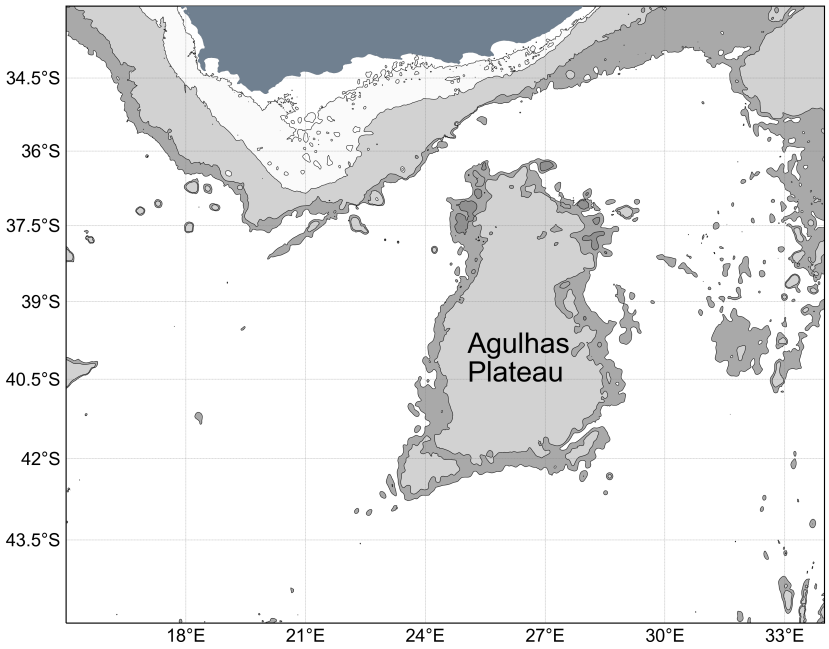

Figure 2.2: Bathymetry of the offshore region south of South Africa obtained from the GEBCO bathymetry data, illustrating the structure and shape of the coastal shelf and the Agulhas Plateau.

2.2 Lagrangian Ocean Analysis

2.2.1 *In Situ* Drifter Observations

Several observational studies are inherently Lagrangian (Lumpkin et al., 2017, Van Sebille et al., 2018, d'Hotman et al., 2019), such as the trajectories of surface drifters, Argo floats and the tracking of marine organisms. Unlike Eulerian measurements which are based on describing fluid motion in a reference frame that is fixed in space as time varies, Lagrangian measurements follow fluid parcels as they move (Van Sebille et al., 2018). Lagrangian measurements provide a more general understanding of the complex flows of the ocean (Van Sebille et al., 2018) meaning it is a valuable method when studying the pathways of the ocean. Surface drifters, also known as surface drifting buoys, are instruments that are designed to follow the water near the ocean surface, thus providing information about the ocean surface currents (Lumpkin et al., 2017).

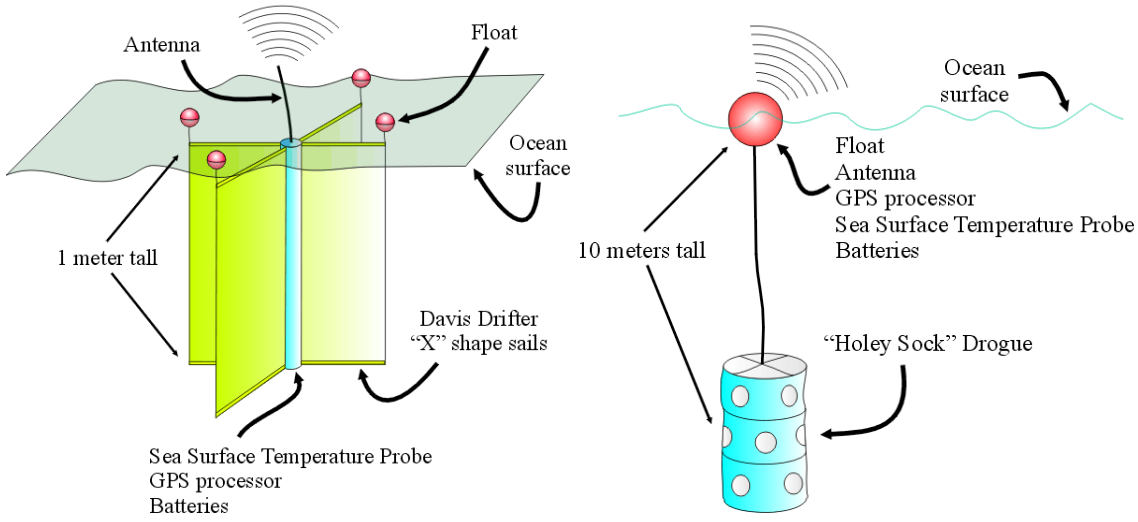

Figure 2.3: An illustration of two different types of drifters known as the Davis drifter (left) and the Holey Sock drifter (right) (King et al., 2002)

Drifters are deployed to serve different functions, from mapping large-scale ocean circulation to following oil spills to aiding in search and rescue operations, which has resulted in the development of a variety of drifter types (Lumpkin et al., 2017) (e.g. Figure 2.3). In general, a drifter is comprised of a surface float and a drogue. Most surface floats contain a transmitter to relay data, a thermometer that reads the temperature and a submerged sensor that detects whether the drogue is still attached or not (over time drifters may lose their drogue). The drogue is generally centred at 15-meter depths (this can vary if the study being done requires a different characteristic) to minimize the direct effects of surface winds so that the trajectory of the drifter is mainly driven by upper ocean currents (Figure 2.4) (NOAA, 2019). Most drifters that are deployed in the global ocean occur as part of the Global Drifter Program (GDP, www.aoml.noaa.gov/phod/gdp/), which forms part of the Global Ocean Observing System (www.aoml.noaa.gov/phod/goos.php). The GDP is designed to provide accurate *in situ* observations of the global ocean. Data obtained from surface drifters have been vital for numerical modellers in providing validation for their model simulations (Barron et al., 2007, van Sebille et al., 2009, Hart-Davis et al., 2018b, Cancet et al., 2019).

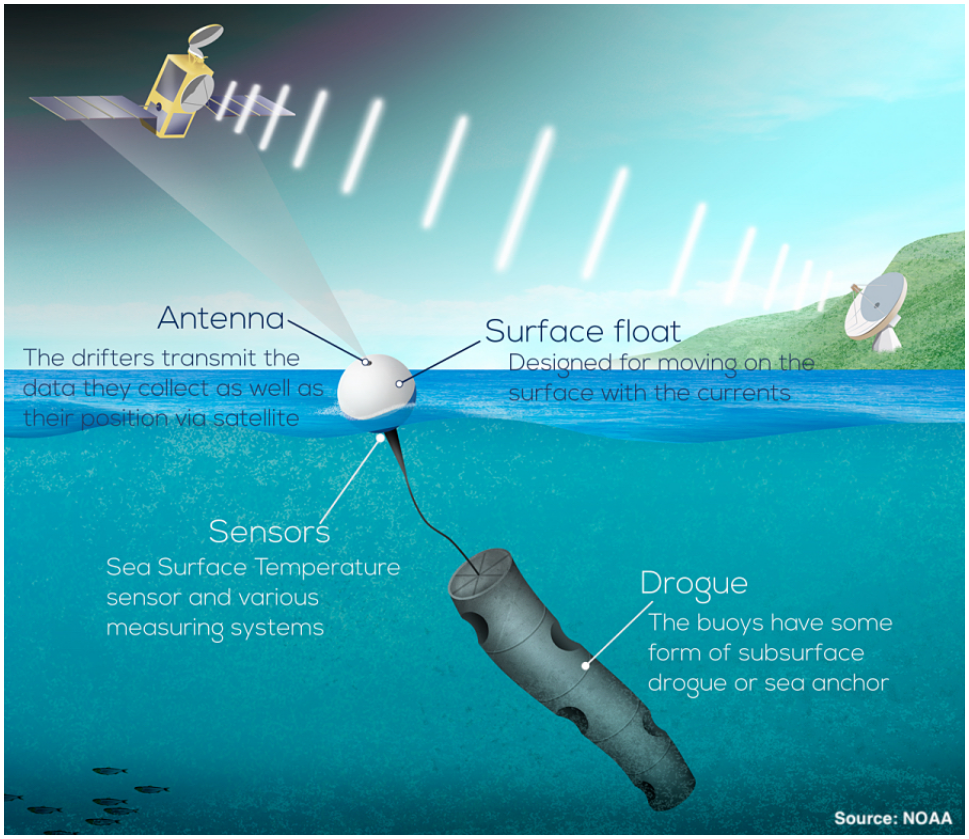

Figure 2.4: An illustration about how a drifter works and how data is transmitted to scientists for real-time use (NOAA, 2019)

2.2.2 Virtual Particle Tracking

Lagrangian ocean analysis through virtual particle tracking within ocean models began in the 1980s (Awaji et al., 1980, Imasato et al., 1980). Since then, virtual particle tracking has been increasingly used by physical oceanographers and marine biologists to study a wide variety of oceanographic processes (Van Sebille et al., 2018, Dagestad and Röhrs, 2019) and applications including larval dispersion (Thorpe et al., 2004, Singh et al., 2018), oil spills (Sayol et al., 2014), hydrodynamic connectivity (van Sebille et al., 2010), microplastic trajectory simulations (Onink, 2018) and search and rescue operations (Breivik and Allen, 2008, Hart-Davis et al., 2018a).

Virtual particle tracking methods are crucial and a powerful tool in the simulation of transport phenomena (Soulsby et al., 2007) and to evaluate sediment transport pathways (Black et al., 2004). Virtual particle tracking has been used in several numerical models to study the dynamics of the Agulhas Current system (Figure 2.1). The dynamics of the Agulhas leakage has been particularly studied using virtual particle tracking to quantify the net mass exchange between the Indian and the Atlantic Ocean (Doglioli et al., 2006, Cheng et al., 2016), to assess the mechanisms responsible for variation in the leakage (Durgadoo et al., 2013) and to assess the connection between oceanic regions (Blanke et al., 2009).

Virtual particle tracking tools fall into two categories: online and offline simulations. The online simulations are calculated along with the velocity fields of oceanic circulation models while the offline simulations take place after the calculations done by the ocean model have been completed (Dagestad et al., 2018). The latter has been increasingly used to allow for the use of several different ocean models when running simulations (Dagestad et al., 2018) and allow for the repeated use of the model outputs with different particle characteristics. As a result of the increased use and broad range of applications, several virtual particle tracking tools have been developed (Figure A.1, A.2 and A.3 of Appendix A).

2.3 Surface Current Components

The surface ocean currents consist of various components, which are governed by different physical processes. These processes include geostrophic currents, Ekman currents, Stokes drift, inertial oscillations and tidal currents. Geostrophic flow in the ocean is a response of the balance between the pressure gradient force and the Coriolis force (Figure 2.5). Geostrophic currents flow along contours of constant dynamic height, with higher dynamic height to the left/right of the flow in the Southern/ Northern Hemisphere (Friedlander, 1980). At larger spatial (>50-100 km) and temporal (>3-10 days) scales the Kuroshio Current, Gulf Stream and Agulhas Current are considered to be geostrophic currents.

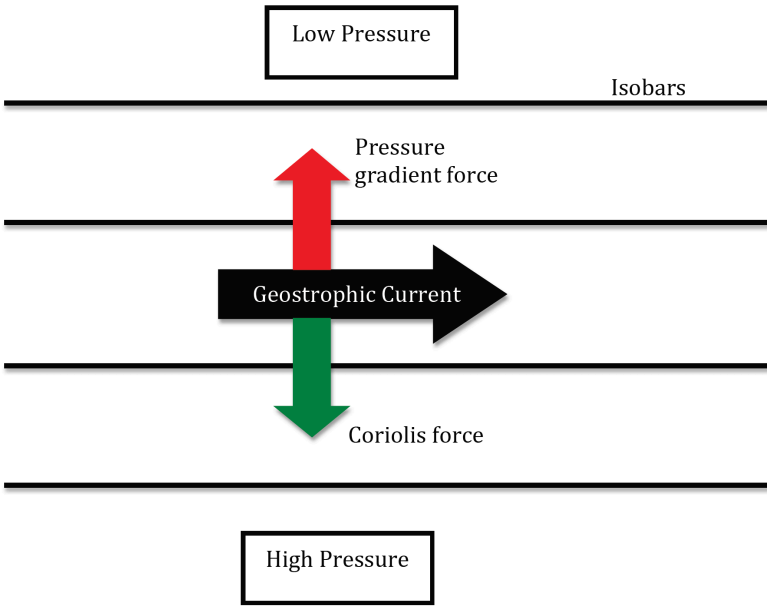

Figure 2.5: A schematic illustrating the resultant geostrophic flow as a response to the balancing of Coriolis forces and the pressure gradient force (Wikipedia, 2019). The deflection to the right of the pressure gradient indicates a flow in the northern hemisphere (as seen in this illustration), while in the southern hemisphere the geostrophic flow is to the left of the pressure gradient.

The lowest-order equations governing such flows are the following simplified equations of motion:

$$v_{geo} = \frac{g}{f}\frac{\delta\eta}{\delta x} \tag{2.1}$$

$$u_{geo} = -\frac{g}{f}\frac{\delta\eta}{\delta y} \tag{2.2}$$

where $f = 2\,\Omega\,sin\phi$ is the Coriolis parameter, with ϕ being the latitudinal position, Ω being the earths rotational velocity and g the gravitational acceleration. The topography of the sea surface, η, is the height of the sea surface relative to a particular level surface (the geoid) (Cushman-Roisin and Beckers, 2011). In certain ocean products, such as GlobCurrent, the η in equations 2.1 and 2.2 are exchanged by the Absolute Dynamic Topography (ADT) obtained from satellite altimeters which allows for the direct estimation of the geostrophic flow of the surface ocean currents.

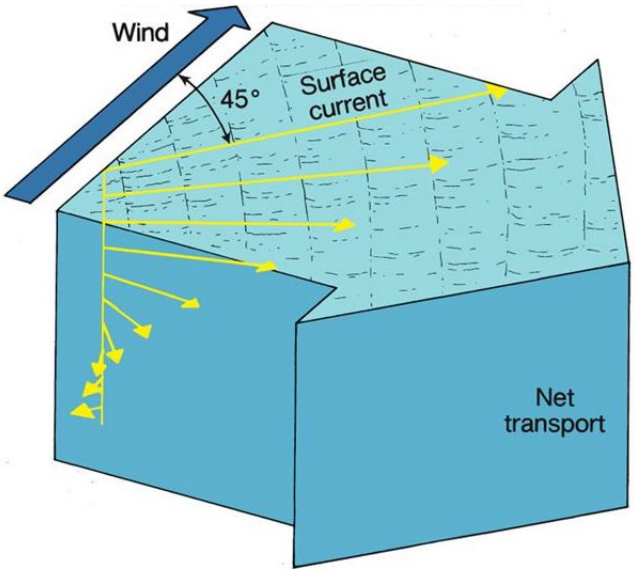

Figure 2.6: An illustration the ocean currents response to the surface wind stress known as the Ekman spiral (Strickland, 2006)

Ekman currents are the response of the ocean currents to the surface wind stress in a rotating frame (Figure 2.6) (Ekman, 1905). Assuming that the ocean is of infinite depth with no boundaries, where the vertical eddy viscosity, A_z, is constant with depth, the balance between the Coriolis force (f) and the induced two-dimensional surface current is:

$$\frac{1}{\rho}\frac{\delta \tau_x}{\delta z} = -f v_{ekman} \tag{2.3}$$

$$\frac{1}{\rho}\frac{\delta \tau_y}{\delta z} = f u_{ekman} \tag{2.4}$$

where u_{ekman} and v_{ekman} are the zonal and meridional Ekman velocities, τ is the wind stress and ρ is the water density (Onink, 2018). In practice, the Ekman currents are estimated using Argo floats and drifter data together with the wind stress from the European Centre for Medium-Range Weather Forecasts (ECMWF) (Rio et al., 2014). At depth z (0 m and 15 m), the Ekman response v_{ek} to the wind stress $\vec{\tau}$ is expressed by (Rio et al., 2014) as:

$$\vec{v_{ek}}(z) = \beta(z).\vec{\tau}.e^{i.\theta(z)}. \tag{2.5}$$

At the surface, the Ekman current is at a 45° angle to the wind stress and going down the water column the magnitude of the current decreases and forms a rotating directional spiral, known as the Ekman spiral (Figure 2.6). The direction of the Ekman spiral relative to the wind stress varies between each hemisphere, with the deflection occurring to the left/right of the wind stress in the Southern/Northern Hemisphere. Unlike geostrophic currents, it is possible for Ekman currents to converge as they are dependent on wind stress and it has been found that Ekman currents are responsible for debris accumulation (Onink, 2018).

Another component of ocean surface currents is Stokes drift, which is induced by the presence of waves and is defined as the difference between the Lagrangian and Eulerian averages of a flow field (Van den Bremer and Breivik, 2017). Physically, as waves travel, the water particles that make up the wave travel in orbital motion (Figure 2.7). Due to the particles spending more time in the forward-moving crest compared to the backwards moving trough, the particle has a net velocity in the direction of the wave propagation, with the net velocity being known as Stokes drift (Van den Bremer and Breivik, 2017). Huang (1979) found that wave motion can influence the dynamics of the surface drift currents and produce a variety of flow patterns ranging from Langmuir circulations to inertial currents. Stokes drift has been shown to have an important impact on the drift of marine debris (Onink et al., 2018) and oil spills (Drivdal et al., 2014). Surface drifters are designed with a drogue (discussed in Section 2.2.1), minimizing the impact of direct wind forcing and the surface wave-driven processes such as Stokes drift (Lumpkin et al., 2017). Another influential factor on the drift of objects in the ocean, is inertial oscillations. Inertial oscillations are a characteristic of the ocean surface layer that arises from the interaction between the wind forcing (u, v) and the Coriolis force (f) (Pollard and Millard Jr, 1970). It is well established that changes in the wind generate inertial oscillations in the surface layer of the ocean (Gonella, 1971, Pollard, 1980). The oscillations in water parcels trace out clockwise circles in the Northern Hemisphere and anticlockwise in the Southern Hemisphere (Talley, 2011) (Figure 2.7).

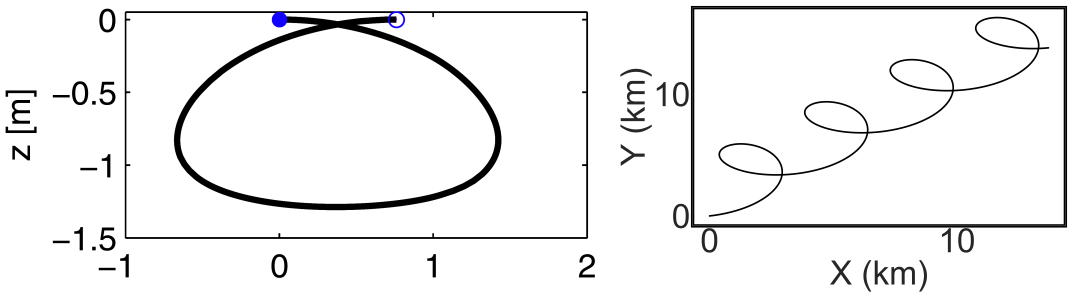

Figure 2.7: An illustration of the impact of Stokes drift, from linear wave theory, of a virtual particle from Bakhoday-Paskyabi (2015) (left). An idealised case illustrating the impacts of inertial oscillations on the trajectory of virtual particles in a two-day experiment (right).

Inertial currents act in both the zonal and meridional plane and are the solution of:

$$\frac{\delta u}{\delta t} = fv \tag{2.6}$$

$$\frac{\delta v}{\delta t} = -fu \tag{2.7}$$

which assumes that advection, pressure gradient forces and dissipation are very small (Talley, 2011).

Inertial periods are often very close to that of tidal periods, so separating the tidal and inertial effects in time series' is difficult. The rise and fall of the tide are accompanied by the horizontal movement of the water, referred to as the tidal current. Tidal currents have periods and cycles (two maximums and two minimums) similar to those of the tides and are subject to similar variations based on the region. The magnitude of the tidal current is correlated with the bottom topography, with large tidal currents being located over shallower regions and reduced tidal currents occurring over deeper regions of the ocean (Poulain and Centurioni, 2015).

Accounting for the effects of gravity waves, tides and inertial oscillations is beyond the scope of this thesis (readers are referred to the following literature for more information: Bakhoday-Paskyabi (2015), Bakhoday-Paskyabi (2016) and Onink (2018)). Therefore, this thesis relies only on the mean ocean surface currents (geostrophic and Ekman currents) to conduct a series of particle tracking scenarios.

2.4 Search and Rescue

Objects go missing in the ocean for a variety of reasons, with the influence of the ocean surface currents depending on the characteristics of the object. Each year numerous incidents, varying from ship sinkings, collisions, recreational and professional marine activities and objects falling overboard, occur in the worlds open oceans and the coastal regions. In South Africa, a significant part of these incidents involve the National Sea Rescue Institute (NSRI) which, in 2017, conducted 1,050 rescue operations (NSRI, 2018). This resulted in the rescuing of 1,224 people and a total of 2,723 hours of operational activity (NSRI, 2018).

To reduce operation times, operation costs and to improve the overall quality of operations, several new and innovative techniques have been developed. In operation, search and rescue is essentially about estimating the search area based on several unknowns and computing the evolution of the search area over time (Breivik and Allen, 2008). These unknowns include physical forces that would act on an object such as winds, currents and waves.

The complexity increases when computing the motion of different objects with varying shapes in the ocean (Breivik and Allen, 2008). Initial techniques looked at the present wind direction and magnitude, making a rough estimation on the position of the object based on the object type and position in the water column. The ability of numerical models to make estimations about the ocean state and wind stress has resulted in these models being increasingly used to estimate the pathway of objects in the ocean. Several tools have been created to account for the type of object to better understand the drift of objects (Breivik et al., 2011, Sayol et al., 2014, Hart-Davis et al., 2018a). The tools presented in Breivik et al. (2011) and Hart-Davis et al. (2018a) independently combine the use of particle tracking and the leeway object divergence methodology presented in Chapter 5 of Allen and Plourde (1999). This method provides an account of how different objects drift in the ocean based on their size and shape as well as their interactions with the physical processes (ocean, windage and waves). Utilizing this methodology allows for a more accurate estimation of the pathways of objects in the ocean and, therefore, can be utilized to speed up operation times and potentially save lives.

2.5 Juvenile Loggerhead Turtles

With the development of electronic tracking and biologging capabilities, the oceanic dispersal of loggerhead sea turtles are a product of passive and active swimming movements (Briscoe et al., 2016). This suggests that the ocean surface components along with the individual swimming behaviour play an important role on the fate of the turtles.

Loggerhead sea turtles (Figure 2.8), Caretta caretta, are distributed widely in the tropical, sub-tropical and warm temperate waters of the global oceans (Barceló et al., 2013). Loggerhead turtles occupy an important position in the food chain, as predators of molluscs, crustaceans and other marine invertebrate species (Machado and Bermejo, 2012). They are known to migrate over long distances, which involves some of the most remarkable feats of navigation and orientation in the animal kingdom (Lohmann and Lohmann, 1996). This is seen when they migrate across the open ocean from their foraging areas to their nesting grounds on their natal beaches (Lohmann and Lohmann, 1996), their birthplace and where they return to reproduce. Adult female loggerheads are known to nest between three to five times per season every two to three years and can lay 105 eggs on average per clutch (Nel et al., 2013). The incubation period for these eggs is between 49 to 69 days (MarineBio, 2019).

Once they hatch, the hatchlings make their way to the ocean at night to avoid predation and the harmful effects of direct sunlight (MarineBio, 2019). The period when hatchling sea turtles disperse from their natal beaches into the ocean are known as the “lost years” (Carr, 1986), as hatchlings disappear into the ocean and are the least understood stage of sea turtle life cycle (Scott et al., 2017). From the point where they enter the ocean, very little is known about the dispersion and behaviour of these hatchlings largely due to animal tracking devices being too large to allow for the tracking of these small organisms (Hazen et al., 2012).

Figure 2.8: Photograph of newly hatched loggerhead sea turtles taken by Ms Diane le Gouvello on a beach in Kwa-Zulu Natal, South Africa.

The proposed life history of juvenile loggerhead turtles suggests that after they swim away from their hatching site, they spend more than a decade in the oceanic environment passively drifting in the ocean currents and only actively swimming for two hours a day (Bolten, 2003b). Studies of the South African loggerhead population Bolten (2003a) and Shamblin et al. (2014) have suggested that a portion of the hatchlings that emerge from the beaches of South Africa enter the Agulhas Current and are then transported by warm water eddies of the Agulhas Current System into the South Atlantic Ocean. The study by Bolten (2003a) modelled the dispersal patterns of South African juvenile turtles under the assumption that they had passive drift. This study suggested that there was a strong likelihood of dispersal of South African juvenile turtles into the South Atlantic but did not find connectivity between the South Atlantic and Indian Ocean basin. However, the assumption that the juvenile turtles are passive drifters is not realistic and the incorporation of their swimming behaviour would have likely had an impact on the results of this study.

3

Data and Methodology

The main focus of this thesis is the development and use of a particle trajectory model in the Agulhas Current system to study the physical processes occurring in the Greater Agulhas Current System. In this section, the tool being used (section 3.1), the ocean surface products (section 3.2) and the Lagrangian parameters (section 3.3) being added to the particle trajectory model will be described.

3.1 Virtual Particle Tracking

Parcels (Probably A Really Computationally Efficient Lagrangian Simulator) is a virtual particle tracking tool aimed at exploring novel approaches for Lagrangian tracking of virtual ocean particles (Lange and van Sebille, 2017, Delandmeter and van Sebille, 2019). The main function of Parcels is to process large datasets generated by contemporary and future ocean general circulation models (Delandmeter and van Sebille, 2019). The framework and interface of Parcels is written in Python, with the computation kernels being generated and compiled in C code during runtime for increased efficiency (Delandmeter and van Sebille, 2019). The structure of Parcels allows for it to be easily adapted for use in a wide range of ocean products and models, which opens up many more applications.

Parcels contains kernels defined for particle advection and types of stochastic motion, but Parcels also allows for the creation of its own kernels that can impact the trajectory of the virtual particles. These kernels can be created to represent a vast number of applications from the trajectory of instrumentation (e.g. Argo Floats, Figure 3.1) to the behaviour of marine organisms to the properties of microplastics. This customizability allows for the use of the tool in a variety of applications such as ocean connectivity (McAdam and van Sebille, 2018), microplastic studies (Duncan et al., 2018, Onink, 2018, Lacerda et al., 2019), larval dispersion (Singh et al., 2018), search and rescue (Hart-Davis et al., 2018a), ocean product validation (Hart-Davis et al., 2018b) and ocean microbial studies (McInnes et al., 2019). Parcels, in the absence of stochastic forcing, computes the Lagrangian trajectories of virtual particles by using the following equation:

$$X(t + \Delta t) = X(t) + \int_{t}^{t+\Delta t} v_{total}(x, \tau)\delta\tau \tag{3.1}$$

where X is the position of the particle, v is the velocity field at location X and τ is equal to t (time at position X) minus t_0 (the initial time of the experiment). Here, the velocity field is composed as $u = u_o + u_a$, where u_o is the ocean surface current and u_a is related to the wind speed.

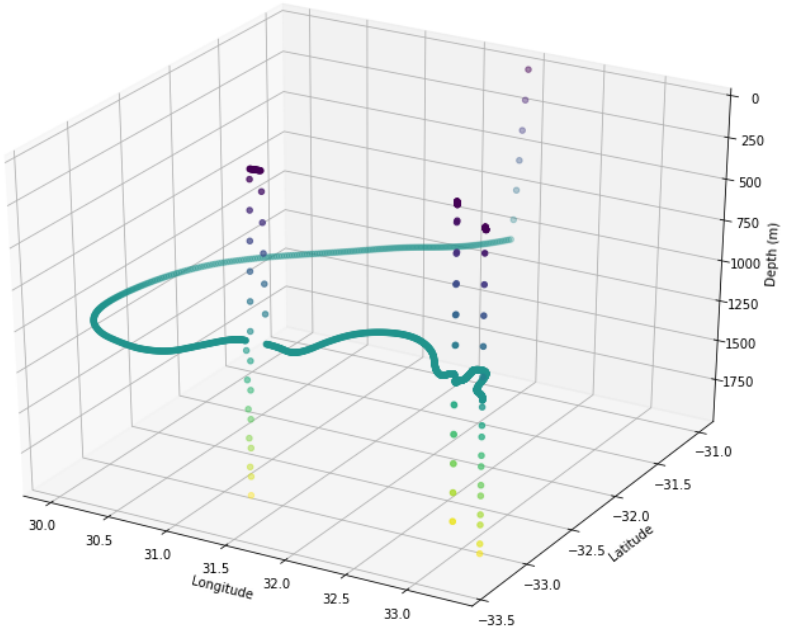

Figure 3.1: An example of a kernel that was made during this Master's thesis that illustrates the trajectory of a "virtual" Argo Float. Here, a simple representation of a virtual Argo float is presented showing how it sinks, remains at a fixed depth (1,000 meters) for 10 days, then sinks down to 2,000 meters before resurfacing. The points are coloured to show the changing depth of the virtual Argo float. The code for this kernel is available at: www.oceanparcels.org.

The u_a can be adjusted to account for the shape and size of the object being studied as shown in Leeway drift model presented in Breivik et al. (2011). In several applications of Lagrangian analysis, an additional term is added at the right-hand side of Equation 2.1 that represents the unresolved physical processes not represented in the velocity fields of the input data. This additional term is represented as $\sqrt{2A_h.\delta t}.\delta W_t$, where A_h and δW_t are the horizontal eddy diffusivity (further explained in Chapter 3.3.1) and a zero-mean white noise random number (Bakhoday-Paskyabi, 2016). Parcels supports the use of input data on a variety of horizontal and vertical grids (Delandmeter and van Sebille, 2019). As previously mentioned, the velocity field can be provided by the output of ocean models or by ocean products. In reality, the v_{total} component is influenced by both the geostrophic current and ageostrophic velocities.

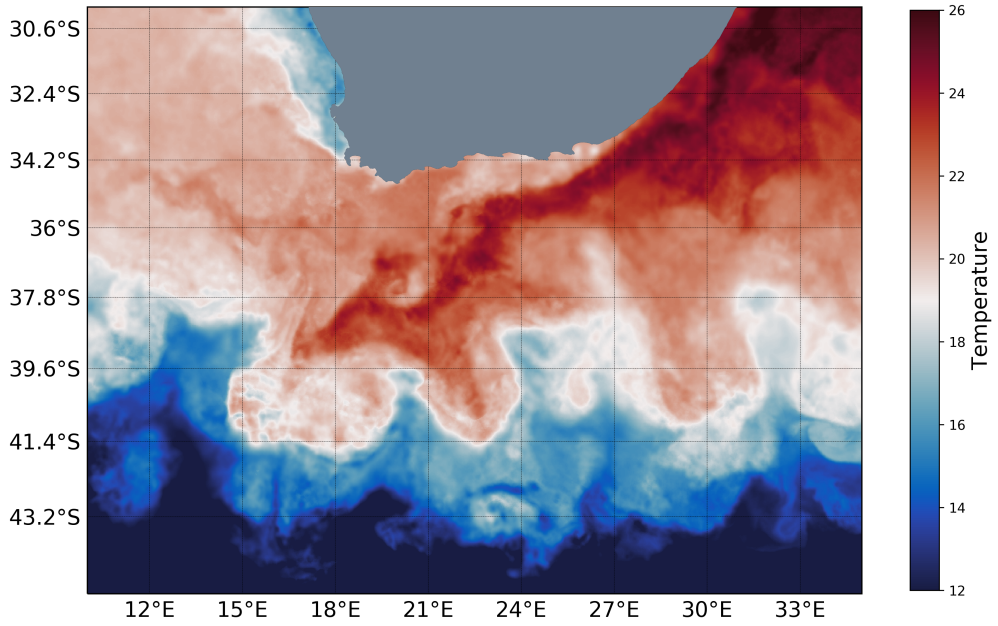

Figure 3.2: A snapshot of the G1SST product illustrating the SST in the Agulhas Current System

3.2 Satellite-Derived Ocean Products

3.2.1 Global 1km Sea Surface Temperature

It has been well established that high-quality global sea surface temperatures (SST) can be produced by blending SST data from multiple satellites and *in situ* observations (Reynolds et al., 2005, Chao et al., 2009). The Group for High-Resolution Sea Surface Temperature (GHRSST) provides a global SST product at a 0.01° by 0.01° spatial resolution and daily temporal resolution from the 9th of June 2010 to the present day (Ocean, 2010). The global 1 km resolution SST (G1SST) (Figure 3.2) product uses satellite data from multiple satellite sensors such as MODIS (Moderate Resolution Imaging Spectroradiometer) and GOES (Geostationary Operational Environmental Satellite), as well as from *in situ* observations from surface drifters and moored buoys (Ocean, 2010). The blended SST fields with a high spatial resolution allows analysis of the structure of fine-scale structures in coastal flow systems (Chao et al., 2009).

A detailed description of the products that are blended together and the technique used to provide the spatial and temporal coverage is given in Chao et al. (2009). Because of its high resolution, compared to GlobCurrent (Section 3.2.2), the G1SST product is used in this thesis to provide additional information about the physical processes of the sea surface for each experiment.

3.2.2 GlobCurrent Ocean Current Product

The GlobCurrent surface ocean currents product is a freely-available (http://www.globcurrent.org/) global ocean dataset provided on a 1/4° spatial grid for the period between 1993 - 2019. The GlobCurrent ocean product v3.0 contains multiple different products consisting of geostrophic currents and Ekman currents provided separately as well as combined at the sea surface and 15-meter depths. The 'total 15-meter currents' product is used in this study to provide a better understanding of the oceanic conditions being experienced by the surface drifters. A more in-depth description of how the total 15-meter currents are derived is presented in Rio et al. (2014). The geostrophic component is derived from maps of satellite altimetry sea level anomalies (SLA), combined with the Mean Dynamic Topography fields (Rio et al., 2013, Cancet et al., 2019). The Ekman currents are estimated using Argo floats and surface drifter observations together with the wind stress provided by the European Centre for Medium-Range Weather Forecasts (ECMWF) (Rio et al., 2014). The GlobCurrent total currents have shown good accuracy in representing large-scale circulation (Lacorata et al., 2019) but have been found to underestimate current velocities of two western boundary currents (Hart-Davis et al., 2018b, Cancet et al., 2019). However, the use of virtual particle tracking with the GlobCurrent total currents is still relevant in studies of upper ocean dynamics. The GlobCurrent data was downloaded from (http://www.globcurrent.org/) and a kernel (see section 3.1) was written for the Parcels tool that extracted the appropriate information from the GlobCurrent data to force virtual particles in the experiment.

3.2.3 Copernicus

The operational Mercator global ocean analysis and forecast system, Copernicus, provides 10-day, 3D global ocean forecasts on a daily basis. This product includes hourly, daily, weekly and monthly mean files of temperature, salinity, currents, sea level height, mixed layer depth and sea ice. The global ocean output files are available at a 1/12° horizontal resolution with regular longitude/latitude equirectangular projection and 50 vertical levels ranging from 0 to 5500 meters.

The ocean model is forced using winds from the ECMWF (European Centre for Medium-Range Weather Forecasts) Integrated Forecast System. The ocean current data are available from the Copernicus Marine Environment Monitoring Service (CMEMS, http://marine.copernicus.eu/). For this thesis, a kernel was created for the Parcels tool that extracts the appropriate temporal and spatial coverage of the CMEMS data, which varied based on the experiment being conducted in the results, directly from the website. Once extracted, a second kernel then calls the required information from the CMEMS data (typically the coordinates as well as the east-west and north-south current velocities) to be used to force virtual particles with the appropriate characteristics for each of the experiments.

3.3 Lagrangian Ocean Analysis

To account for the complexity of the motion of particles in the ocean, certain parameters can be added to the equation to give a more realistic representation of the particle's motion. These added parameters are themselves complicated and require justification depending on the application and processes that are trying to be resolved. In the next two sections, two of these parameters, stochastic motion (section 3.3.1) and boundary conditions (section 3.3.2), are presented.

3.3.1 Stochastic Motion

Turbulent processes, such as mesoscale (10 - 100 km) eddies and jets, cause virtual particles to disperse quickly and increase the rate of mass, momentum and tracer spreading, leading to accelerated mixing (LaCasce, 2008). Lagrangian eddy diffusivity is introduced to quantify the rate of dispersion related to the cumulative effect of eddies (Rühs et al., 2018) and to account for the unresolved physical (sub-grid scale) processes not represented in the ocean models (Van Sebille et al., 2018). Several different techniques are added to particle tracking tools to account for these processes (see Figure A.1, A.2 and A.3 of Appendix A). The most commonly used method is Brownian motion, which is also an optional kernel in Parcels.

Brownian motion (Hida, 1980) uses horizontal eddy diffusivity (K) and is applied to account for the unresolved processes in the particle trajectory model. The implementation of diffusion is important in the field of research in the ocean Lagrangian community and cannot be neglected (Delandmeter and van Sebille, 2019). The estimation of the horizontal eddy diffusivity is challenging and there are several different formulations that have been presented (Taylor, 1922, Davis, 1991, Visser, 1997, LaCasce et al., 2014, Zhurbas et al., 2014, Van Sebille et al., 2018, Rühs et al., 2018). Horizontal Lagrangian eddy diffusivity can be estimated from both single-particle and pair-particle statistics (LaCasce, 2008). Here, three different techniques are presented that were used or developed to be used in Parcels for the use in applications presented in this thesis (Section 4.1, 4.2 and 4.3).

1. The first and the most basic technique is the use of a single fixed value to represent the average horizontal eddy diffusivity of a domain or region. In this case, a fixed value is calculated from *in situ* observations (Bogucki et al., 2005) or a single mean value is extracted from a numerical model output (Rühs et al., 2018). This technique is much quicker than other techniques but it neglects the fact that horizontal eddy diffusivity varies both spatially and temporally. However, this technique still provides a better representation of processes affecting the trajectory of virtual particles in the ocean compared to simply using passive particles.

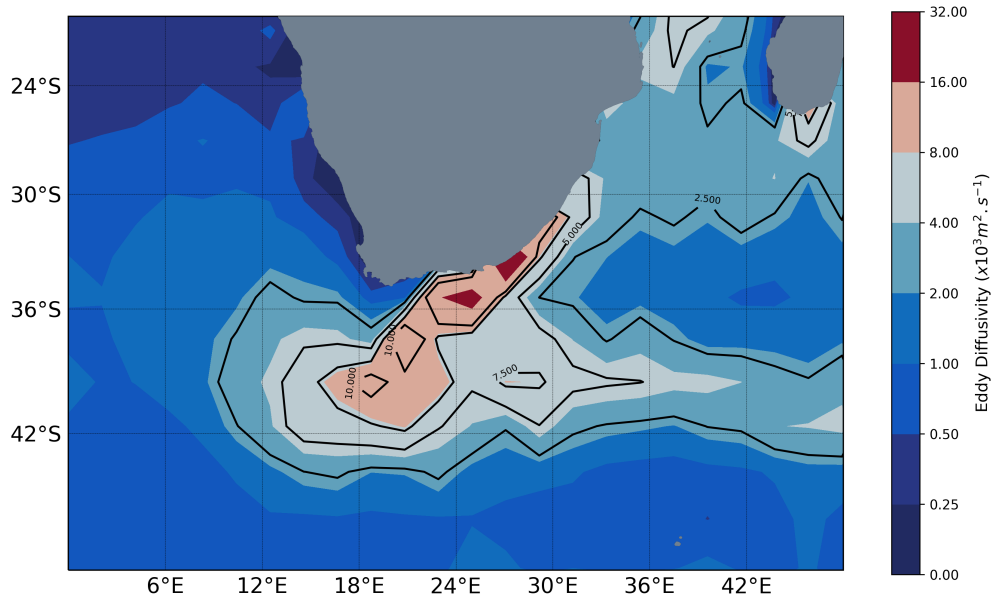

Figure 3.3: Surface horizontal eddy diffusivity calculated from surface drifters deployed between 1993 and 2017 using the methodology presented in (Oh et al., 2000, Zhurbas et al., 2014, Rühs et al., 2018).

2. The second technique is to calculate the horizontal eddy diffusivity directly from surface drifter observations. *In situ* observations provided by satellite-tracked drifting buoy data, provide a good coverage of the global ocean and can be used to study horizontal Lagrangian eddy diffusivity. However, due to the limited number of drifter pairs that have been deployed, a particle-pair approach cannot yet be used to calculate a spatially varying horizontal diffusivity (Oh et al., 2000). Therefore, the most popular way of extracting horizontal diffusivity is from single-particle statistics (Taylor, 1922, Oh et al., 2000). The approach of estimating eddy diffusivity presented in Rühs et al. (2018), was first introduced by Oh et al. (2000) and further improved by Zhurbas et al. (2014) to account for mean flow suppression of eddy diffusivities. This eddy diffusivity estimation involves three steps: a) binning of particle (surface drifter) trajectories on a longitudinal-latitudinal grid; b) estimation of the mean flow, Lagrangian velocities and displacement; and c) estimation of the ensemble-mean eddy diffusivities for each bin (Rühs et al., 2018).

In Figure 3.3, the domain is divided into 0.5° × 0.5° grids and each drifter that passed through the ocean surrounding Southern Africa between 1993 to 2016 was considered. Only drifter trajectory segments where the drogues were still attached to the drifter were considered. This is due to drogued drifters being designed to remain at a fixed depth and once the drogue has been lost, the drifters' vertical position can vary considerably. Once the drifter data was extracted, the approach introduced by Zhurbas et al. (2014) and Rühs et al. (2018) was followed to calculate the eddy diffusivity, $K(x;t)$, as seen in Figure 3.3.

The single-particle diffusivity tensor, following (Davis, 1991), is defined as:

$$k_{jk}(x,t) = -\langle v'_j(t_0|\vec{v_x},t_0).d'_k(t_0-t|\vec{v_x},t_0)\rangle, \tag{3.2}$$

where v' and d' are the departures from the Lagrangian mean velocity and displacement respectively. The notation $(t_0|x,t_0)$ represents the value of v'_j and d'_k at time t of a particle passing through $\vec{v_{x0}}$ at time t_0 (Oh et al., 2000). t_0 is the initial time point t and the square brackets designate particle ensemble averaging (Zhurbas et al., 2014). Following Swenson and Niiler (1996) and Oh et al. (2000), the diffusivity is calculated as follows:

Every data point in each grid cell is considered as the initial point of a pseudo-trajectory with all values of time yielding a displacement dt as a function of time as well as individual value of velocity $v(t_0)$ at the origin. By ensemble averaging, the mean values of displacement $D(t)$ and velocity $U(t_0)$ are obtained, meaning the departures, $d'(t) = d(t) - D(t)$ and $v'(t_0) = v(t_0) - U(t_0)$, can be estimated. The diffusivity k_{jk} is then estimated as the mean product of the departures from the displacement and velocity, $v'(t_0).d'(-t)$.

The next step in the methodology introduced by (Oh et al., 2000, Zhurbas et al., 2014) is the decomposition of the diffusivity tensor into symmetrical and asymmetrical components $k^S_{jk} = (k_{jk} + k_{kj})/2$ and $k^A_{jk} = (k_{jk} - k_{kj})/2$. The symmetrical and asymmetrical components are respectively describing the growth of the particle dispersion (i.e. the diffusion) and the rotation of the particle ensemble (Zhurbas et al., 2014).

To avoid rotational eddy fluxes, which are non-diffusive, only the symmetric part of k_{jk} is considered, which will now be referred to as k_{jk}^{davis}. The lateral diffusivities may also be assessed as half of the growth rate of the Lagrangian particle's dispersion tensor s_{jk} (Zhurbas et al., 2014):

$$k_{jk}^{disp}(x,t) = \frac{1}{2}\frac{\delta s_{jk}}{\delta t}; \tag{3.3}$$

with

$$s_{jk}(x,t) = \langle d'_j(t_0+t|x,t_0).d'_k(t_0+t|x,t_0)\rangle. \tag{3.4}$$

whereby the notation $d'_k(t_0+t|x,t_0)$ represents the kth component of the residual displacement of a particle passing through x at time t_0, obtained from the forward trajectory of particles in time for the period $[t_0, t_0+t]$ (Rühs et al., 2018). Oh et al. (2000) showed that the minor principal components of k^{disp} and k^{davis} are less biased by shear flow.

Therefore, combining the two frequently used approaches for diffusivities estimations:

$$K(x,t) = [k^{davis}(x,t) + k^{disp}(x,t)]/2, \tag{3.5}$$

yields a spatially and temporally varying horizontal eddy diffusivity $K(x,t)$ (Rühs et al., 2018). This technique utilizes the realistic representation of the ocean dynamics provided by the drifter observations to present a spatially/temporally varying representation of horizontal eddy diffusivity. However, due to the low frequency of drifter observations, a climatology of all the drifter observations needs to be created to fill in the regional gaps in the data. This climatology provides a better representation than fixed eddy diffusivity. However, the fixed temporal resolution restricts the accuracy of horizontal eddy diffusivity compared to reality. This technique of estimating horizontal eddy diffusivity from drifter observations is implemented by this thesis into the Parcels tool for use in section 4.1.

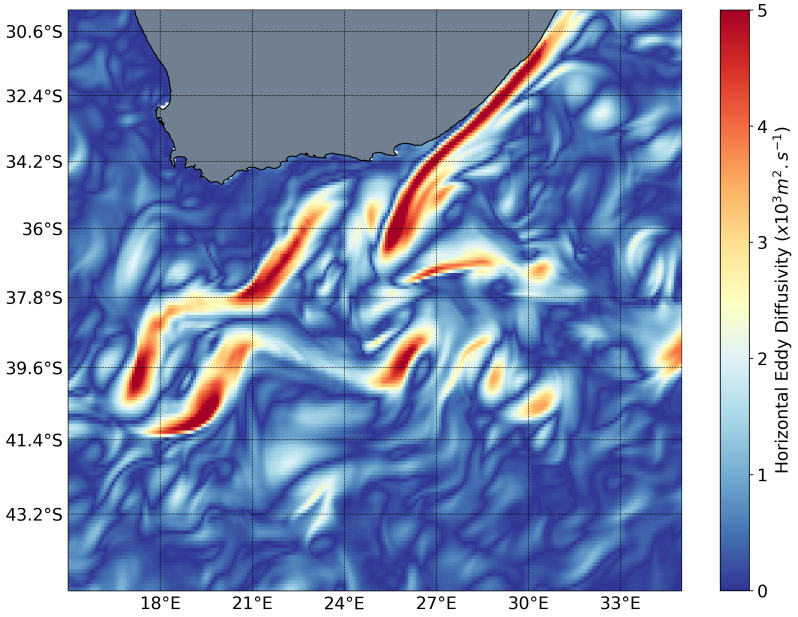

Figure 3.4: An example of the surface horizontal eddy diffusivity extracted from a simulation run using the Regional Ocean Modelling System (ROMS-Agrif)

3. To account for the spatial as well as temporal variation, the horizontal eddy diffusivity can be calculated from numerical ocean model simulations, either online during the model run or offline after the model run. In most cases, running a numerical model simply to get the online estimation of horizontal eddy diffusivity (such as in Figure 3.4) is inefficient based on the time it takes to run and the process of validation of the numerical model results. The offline calculation, on the other hand, allows for the use of multiple numerical models.

This technique gives a spatially and temporally varying horizontal eddy diffusivity that will provide the best representation of the unresolved physical processes. Although this technique is limited by the spatial and temporal resolution as well as the inherent capabilities of the numerical model, it is considered to be the best option. The technique used to calculate the horizontal eddy diffusivity from the numerical model output in this thesis is the baseline Smagorinsky model based on Smagorinsky (1963) and Lévêque et al. (2007). The Smagorinsky model is the simplest and most commonly used eddy viscosity model (Lévêque et al., 2007) with the major benefits being the manageability, the computational stability and the simplicity of its formulation. The horizontal eddy diffusivity (v_T) is calculated as follows:

$$v_T(x,t) = (C_s\Delta)^2|\overline{S}(x,t)|, \tag{3.6}$$

where $|\overline{S}| \equiv (2\overline{S}_{ij}.\overline{S}_{ij})^{1/2}$ represents the magnitude of the resolved rate-of-strain and C_s is a non-dimensional coefficient (called the Smagorinsky constant) Lévêque et al. (2007). In this thesis, this capability is introduced into the Parcels framework in the form of a kernel that extracts all the appropriate information from the ocean surface product to calculate the horizontal eddy diffusivity. This technique is used in section 4.1, 4.2 and 4.3.

3.3.2 Boundary Conditions

The addition of the stochastic terms in the calculation of particle trajectories, enables the particles to encounter the boundaries more frequently (Carlson et al., 2010). If a stochastic 'jump' results in a particle reaching a boundary, that particle is temporarily 'stuck' on the boundary (Carlson et al., 2010) or the particles may move onto land. These particles may enter the ocean in future time steps through a stochastic motion which is comparable to floating debris being deposited onto a beach through wave action and possibly being swept back out to sea (Carlson et al., 2010). In applications where this process of particles getting 'stuck' is not realistic, different boundary conditions should be implemented that give a more realistic representation of what is expected.

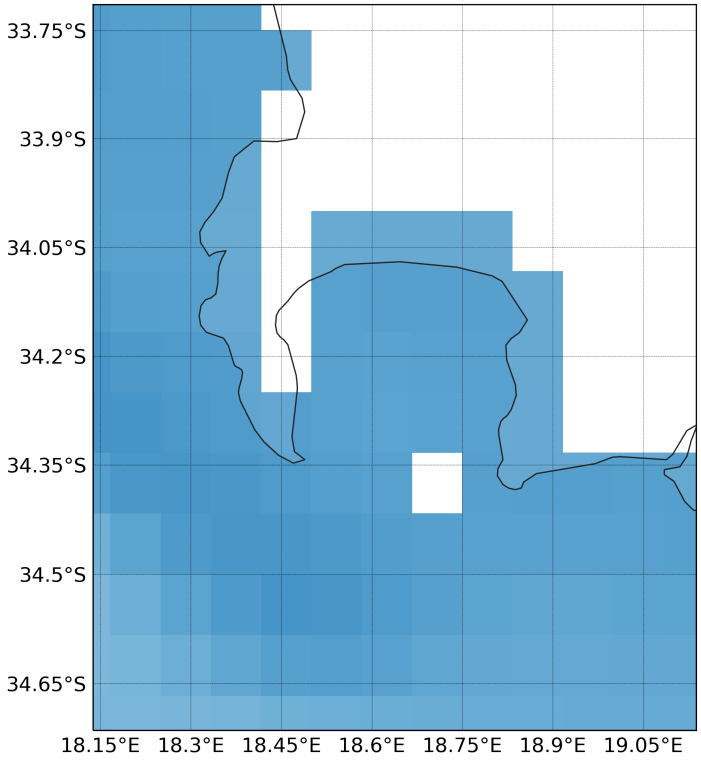

Figure 3.5: An illustration of the coastline of False Bay, South Africa represented by reality (the black line) and how a numerical model represents the land-sea boundary (in this case showing a CMEMS model output).

For example, some applications require that particles do hit the land boundary and stop (marine organism studies), whereas in other applications it is not realistic for particles to hit land (ocean dynamics studies). With the limitations of numerical models to properly represent the characteristics of the coastal regions (Figure 3.5), the pathways of particles in these regions are poorly represented and it is, therefore, important to develop different boundary conditions that can be used for the different applications.

The use of the particle trajectory model, in this thesis, is to simulate two-dimensional applications, with no vertical boundaries being included. It should be noted that there are applications where boundary conditions will need to be implemented at the border of the numerical model domain, however, in this thesis particles will be discarded from the study at the point where they leave the domain.

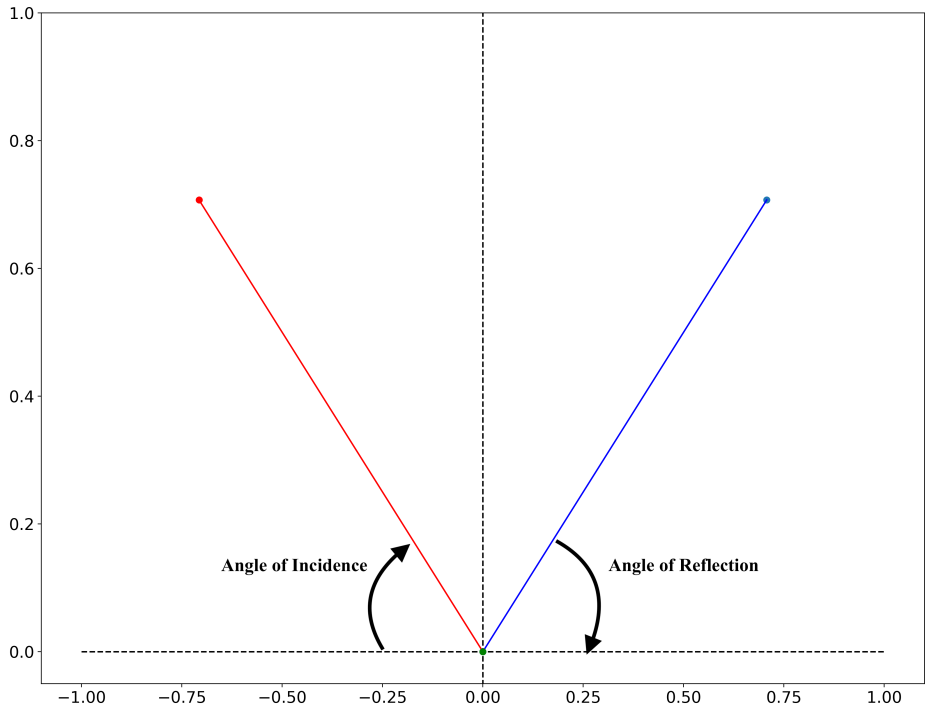

Figure 3.6: A simple schematic showing the basic concept of reflection of a virtual particle off a boundary. The red line represents the particle trajectory prior to reaching and hitting a boundary (at the angle of incidence). The green circle represents the position where the virtual particle would hit the boundary. The blue line is the resultant trajectory of the virtual particle once reflected off the boundary (at the angle of reflection).

Reflective Boundaries

One of the possible boundary conditions is reflective boundaries. Weitbrecht et al. (2004) implemented reflective boundaries in their study of particles travelling down a river to prevent the particles from leaving the domain. In this study, particles that would cross the upper or lower boundary at a certain time step were reflected into the domain of study (Weitbrecht et al., 2004). A schematic is shown in Figure 3.6, illustrating the basic concept of reflection, where a particle hitting a boundary is then reflected into the domain. The implementation of reflection becomes more complex when you take into account the shape of the coastline as this will have an impact on the angle of reflection.

Reflection based on the real coastline is more representative of reality than reflection based on the numerical model boundaries due to their boundaries being rectilinear (as seen in Figure 3.5). Reflective boundaries based on the shape of the coastline have been developed in this thesis for the Parcels tool and are used in Subsection 4.1 and 4.2 of this thesis.

Dead Zones

When conducting particle trajectory modelling studies on marine organisms, it is important to take into consideration the dominant oceanic properties (such as temperature and salinity), where it is expected that organisms would not be able to survive.

In some studies, such as larval dispersion or migration of marine organisms, when particles hit a boundary (such as the coast) it is expected that particles will become stuck at the boundary. Furthermore, the physical properties of the ocean may have an impact on whether the marine organisms survive or not. Hence, when conducting particle trajectory modelling studies on marine organisms as they encounter oceanic properties where they would not survive, such as colder or toxic water, it is necessary to remove the particles from further trajectory simulations. In this thesis, so-called 'dead zones' are implemented which removes virtual particles when they hit regions where the object being studied is not expected to survive and records their final position. The 'dead zones' have been developed and implemented into the Parcels tool and are used in the study of the juvenile turtles in Section 4.3.

4

Results

In this section, results are presented from a series of idealized and realistic experiments. As described in Chapter 1, these experiments have been designed to specifically investigate three key focus areas. Firstly, the effects of changing different influential parameters in the particle trajectory model are investigated (section 4.1). Following this, the particle trajectory model is used to study drifter separation in the Agulhas Current from drifter buoys observations (section 4.2) and finally, to evaluate the importance of initial swim speeds on juvenile turtle dispersion (section 4.3). These results highlight the diverse application of the particle trajectory model, as well as the importance of ensuring the correct parameters are used, especially in regards to the final application of the model.

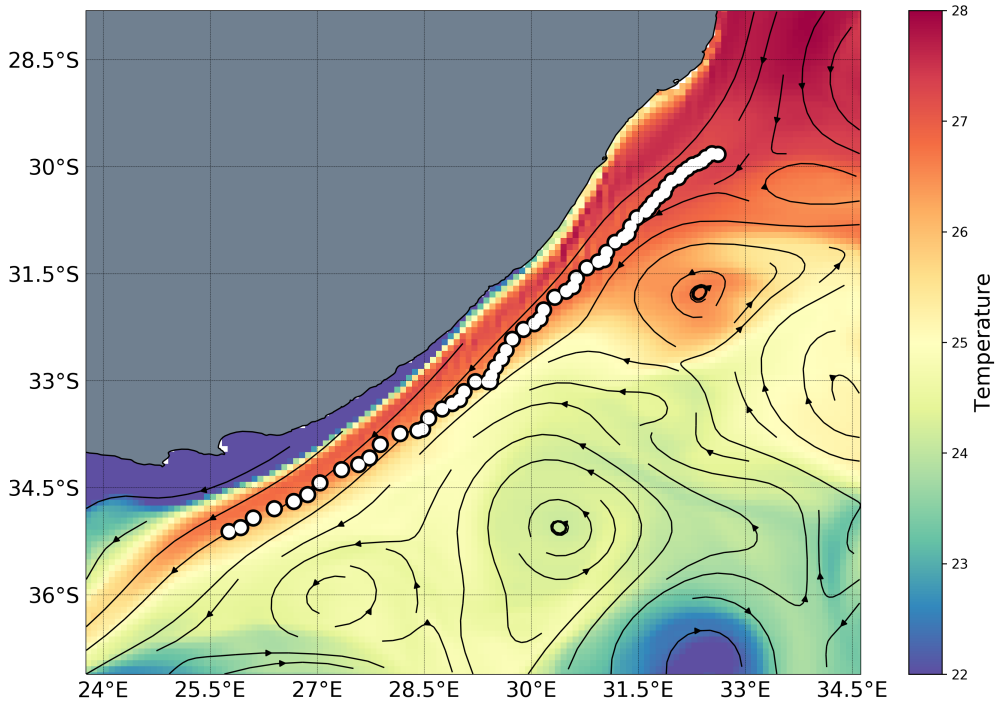

Figure 4.1: The 6-hourly position of the real surface drifter 101808 (white dots) overlaid onto a weekly-mean SST fields (9th to 16th of February 2014) and ocean surface current streamplots obtain from the CMEMS ocean product.

4.1 Lagrangian Ocean Analysis

In both subsection 4.1.1 and 4.1.2, the trajectory of a surface drifter buoy deployed as part of the GDP program (drifter 101808, Figure 4.1) is used to assess the ability and impact that the developed parameterizations have on the virtual particle trajectory. Drifter 101808 was chosen as it moves relatively close to the coast, which means there is a possibility that the virtual drifters used to imitate the drifter trajectory will get closer to the land-sea boundary and can, therefore, be used to assess boundary parameterizations. The drifter was initially deployed on the 10th of December 2013 at 38.720° E and 26.919° S but passes through the region illustrated in Figure 4.1 between the 9th and 16th of February 2014. Subsection 4.1.1, will assess the impact of stochastic motion, subsection 4.1.2 the impact of the boundary conditions and 4.1.3 the parameters in search and rescue applications.

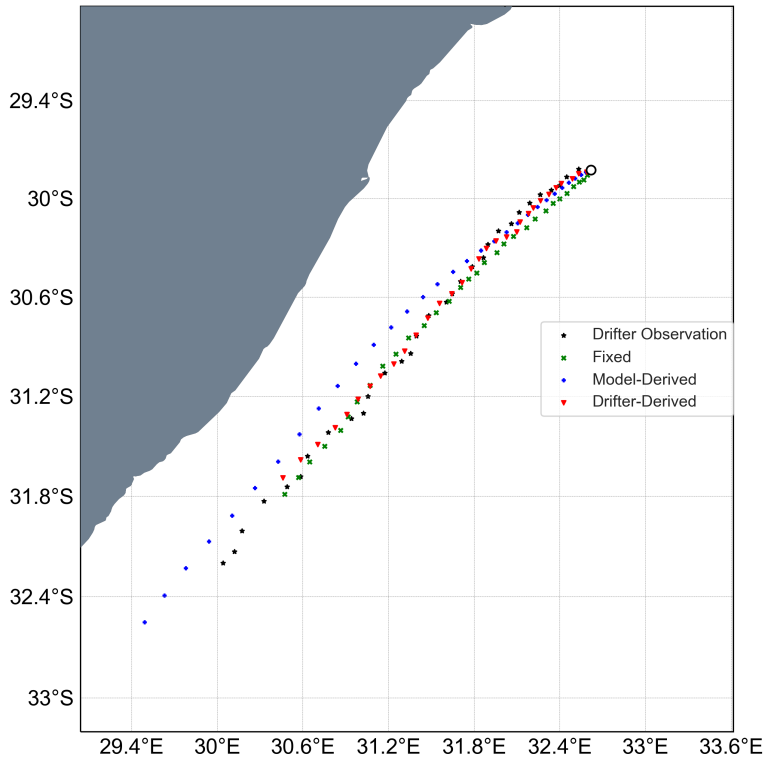

Figure 4.2: Trajectories for the observed (black) and virtual drifters for each of the experiments conducted. Only the mean trajectory of the virtual drifters from each experiment is shown.

4.1.1 Stochastic Motion

Three different experiments were conducted to assess the impacts of stochastic motion and horizontal eddy diffusivity on the trajectory of virtual drifters compared to the observed drifter. For each experiment, 1000 virtual drifters were deployed for eight days (Figure 4.2) into the ocean surface currents from the CMEMS ocean product (Section 3.2.3). The experiments were divided as follows: the first experiment used a fixed value for horizontal eddy diffusivity of 400 $m^2 s^1$; the second had a spatially varying horizontal eddy diffusivity extracted from a drifter data climatology (Figure 3.3); and the third had spatially and temporally varying horizontal eddy diffusivity calculated from the ocean product input data using the baseline Smagorinsky model (Smagorinsky, 1963, Lévêque et al., 2007).

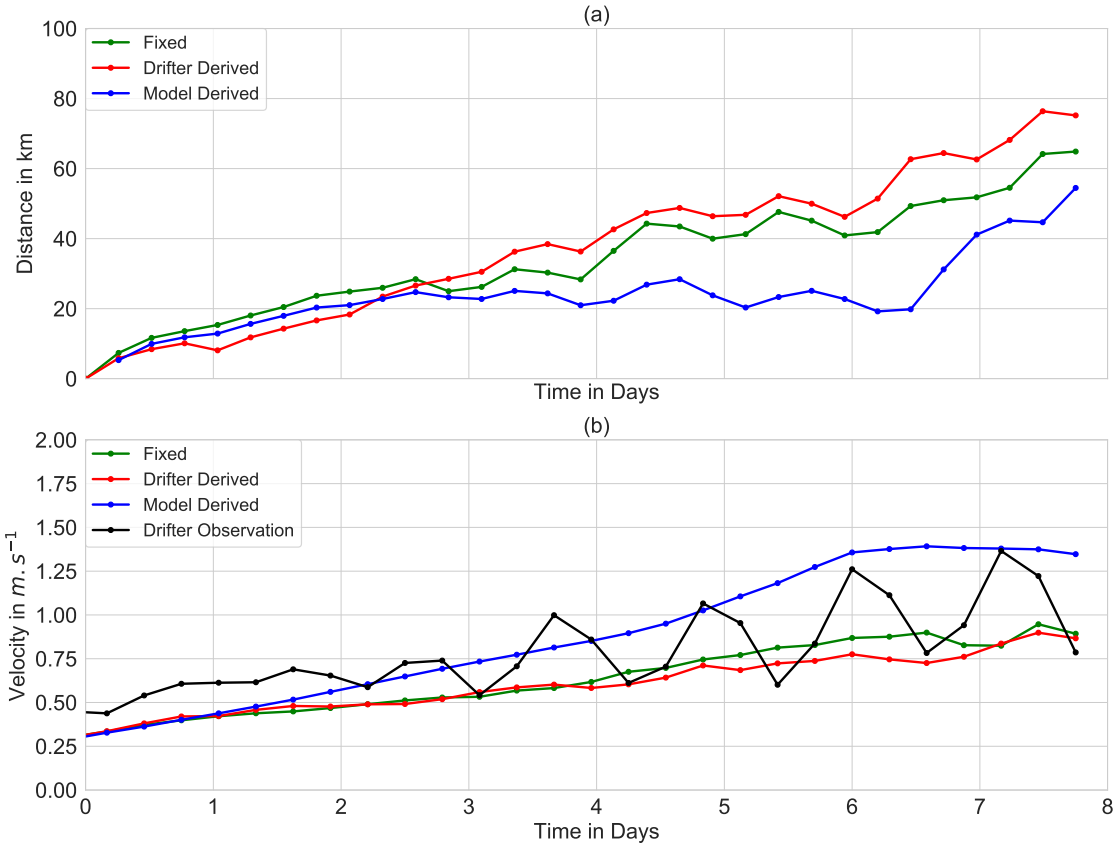

Figure 4.3: The distance between the observed surface drifter and the mean virtual drifter positions over time (a) and the velocity of the virtual and observed surface drifter at each time step (b) is also presented.

As shown in Figure 4.2, the virtual drifters and observed drifter show a similar trajectory. Given that the movement of the virtual drifters is only driven by the surface currents, it can be assumed that the Agulhas Current jet is driving the trajectory of the surface drifter (Figure 4.1 and 4.2). In the first two days of the experiment, all CMEMS forced virtual drifters underestimate the velocity of the observed surface drifter, which explains the initial increase in distance separation (Figure 4.3). For all the virtual drifters, the mean velocity is relatively stable compared to that of the observed drifter which shows a lot of fluctuations in the mean velocity. This lack of fluctuation in the virtual drifter velocities explains as to why there is separation from the observed surface drifter positions.

Furthermore, this indicates that the CMEMS surface currents are not properly resolving the physical processes being experienced by the observed drifter. The distance separation between real and virtual drifters of the drifter-derived horizontal eddy diffusivity performs the best of all the experiments in the first two days. However, after three days the drifter-derived horizontal eddy diffusivity performs the worst and the model-derived horizontal eddy diffusivity becomes the best performing method (Figure 4.3). The distance separation between the model-derived horizontal eddy diffusivity remains relatively constant at between 20 – 30 km from day two to just after six days. The spatially and temporally varying model-derived horizontal eddy diffusivity reduces the separation distance between the observed surface drifter and virtual drifter to, on average, 2.99 km per six-hour time step from 3.40 km for the drifter-derived and 3.80 km for the fixed horizontal eddy diffusivity. These results suggest that in studies comparing virtual and observed drifters, using model-derived horizontal eddy diffusivity provides a better representation of the physical processes not being resolved by numerical model outputs.

4.1.2 Boundary Conditions

To assess whether boundary conditions have an impact on the resultant trajectory of the virtual drifters, three experiments were set up to test the different boundary conditions. The experiments were divided as follows: the first experiment having no added boundary conditions; the second having reflective boundaries; and the third having 'dead zone' boundaries (removing particles from the study when they interact with the boundary). For all of the experiments, the fixed value horizontal eddy diffusivity parameter (of 400 $m^2 s^{-1}$) was applied. As in the previous section, the virtual and observed surface drifters show a similar trajectory pattern which suggests little variation in the path of the current (Figure 4.4). Although the mean trajectory of the virtual drifters does not demonstrate an interaction with the boundaries when looking at all of the virtual drifters (grey lines in Figure 4.4) some do interact with the boundaries. This is due to the addition of the stochastic terms resulting in the virtual drifters 'jumping' towards the boundary (Carlson et al., 2010). Therefore, applying the boundary conditions (introduced in Subsection 3.3.2) will have an impact on the mean trajectory of the virtual drifters in this experiment.

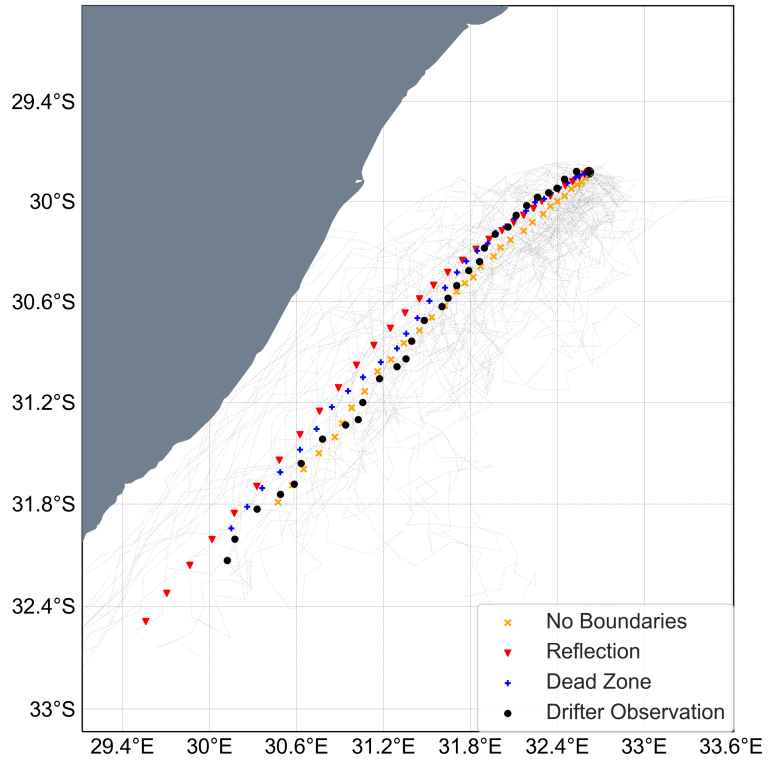

Figure 4.4: The trajectory of the observed surface drifter observation (black) and the virtual drifters from each of the boundary condition experiments conducted. The grey lines represent all 1,000 of the virtual particles that were deployed in the reflection experiment only, with the coloured trajectories representing the mean of the experiments.

The velocity of the virtual drifters still does not properly represent the velocity of the surface drifter, which rationalizes the significant separation between the observed and virtual drifters over time. However, the velocity of the 'dead zone' and reflective boundary virtual drifters moves closer to that of the surface drifter explaining why both boundary conditions produce less distance separation over time. As seen in Figure 4.5, both of the boundary conditions improve the distance separation of the virtual drifters from the surface drifter over time, with no boundaries resulting in an average of 3.40 km separation per six-hour time step while 'dead zones' and reflective boundaries result in a 3.24 km and 2.88 km distance separation respectively.

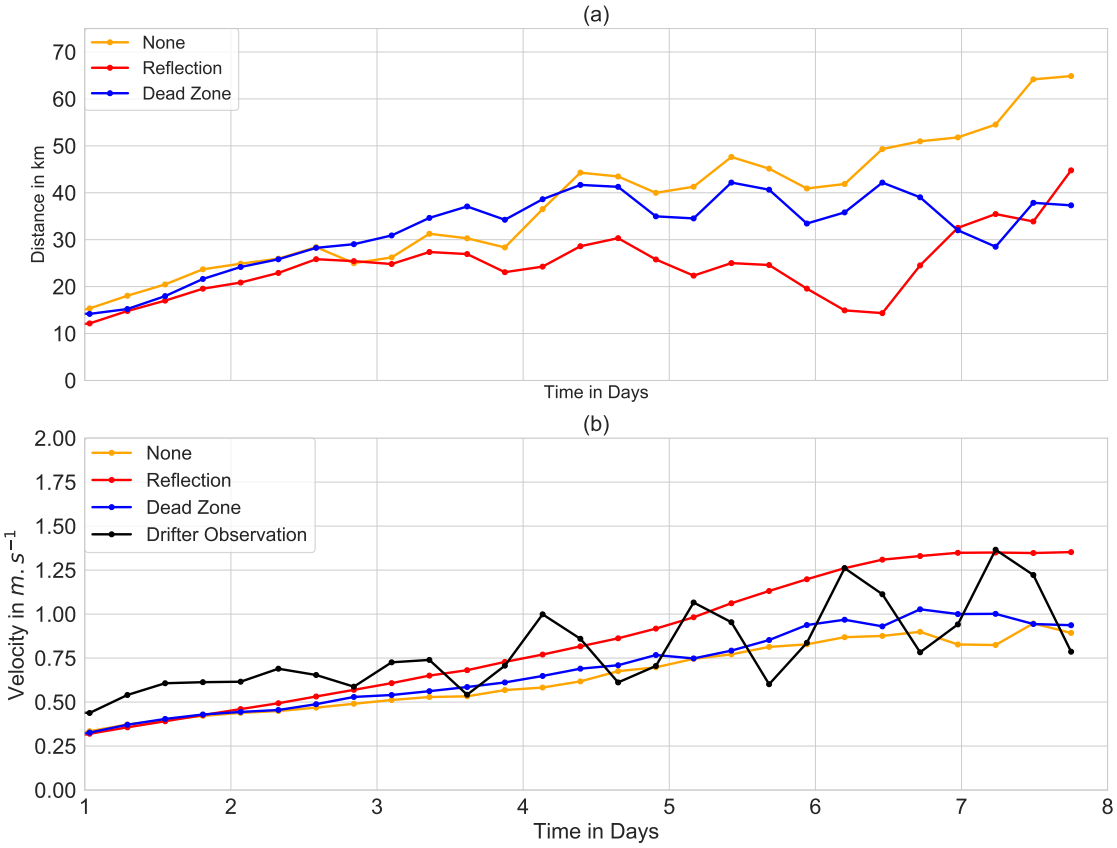

Figure 4.5: The distance between the observed surface drifters and the mean virtual drifter positions over time (a) and the velocity of the virtual and observed surface drifter at each time step (b) is also presented.

Therefore, including boundary conditions improves the virtual drifter accuracy in representing the trajectory of a surface drifter. Furthermore, the reflective boundary provides a greater improvement in the accuracy of virtual drifters in representing the surface drifter trajectory compared to a 'dead zone' boundary. However, it is important to note that boundary conditions should be chosen carefully based on applications and studies that are being conducted.

4.1.3 Search and Rescue

To test the hypotheses highlighted in Section 4.1.1 and 4.1.2, the particle trajectory model was used in a real search and rescue experiment of a capsized catamaran. On the 18th of January 2016, the upturned hull of a catamaran was spotted approximately 113 Nautical Miles off Cape Recife (25° 41' 59.46" E and 34° 24' 11.08"S), near Port Elizabeth (South Africa), which was first reported missing a year earlier, in January of 2015. Five days later, on the 22nd of January 2016, the National Sea Rescue Institute (NSRI) found the capsized catamaran south of Cape Agulhas (20° 07' 32.58"E and 35° 01' 31.94"S). The positions of the capsized vessel provide valuable information that can be used to address the shortcomings of the particle trajectory model developed in Hart-Davis et al. (2018b) and Hart-Davis et al. (2018a). An approach is presented to assess the accuracy of using a particle trajectory model that combines predicted surface ocean current velocities, 10-meter winds, 'dead zone' boundary conditions and stochastic motion to estimate the path of the capsized vessel. Windage was added to the virtual particles based on the Leeway drift model presented in Breivik et al. (2011) to account for the shape and size of the vessel, in this case a capsized catamaran. The 'dead zone' boundary condition is used in this application as it is expected that when a capsized vessel hits the coast that it will beach. The analyses in Hart-Davis et al. (2018b) are restricted to the conditions when there is no interaction between wind and current, such as in the absence of spatial variability of turbulent forcing. For all of the following experiments, 1000 virtual particles were deployed for five days starting on the 18th of January 2016 at the last known position of the capsized vessel (25° 41' 59.46"E and 34° 24' 11.08"S). In the horizontal eddy diffusivity experiments, the use of four different fixed horizontal eddy diffusivities in calculating the stochastic motion, Brownian Motion (Hida, 1980) are investigated with the 'dead zone' boundary condition. In the virtual particle forcing section, a series of virtual particle experiments are conducted to investigate the importance of combining wind and surface currents in an example of a capsized vessel. For all experiments, the ECMWF 1/10° daily mean winds and/or the 1/12° Mercator ocean surface velocity data was used. The information of wind and surface currents were calculated along the particle trajectories using bilinear interpolation for all the experiments done in this study.

Table 4.1: . Summary of the results of the simulations using four different fixed values of horizontal eddy diffusivity. The mean Lagrangian displacement was calculated by the formula adapted from (LaCasce, 2000) : $M_x(t) = 1/N(x_t - x_o)$. Where N is the number of particles, x_t is the position of particles at time t and x_o is the initial position of the particles.

Fixed Horizontal Eddy Diffusivity ($m^2.s^{-1}$)	Percentage of particles that hit the coast	Furthest particle from recovery point of vessel (in km)	Percentage of particles that passed through the bin of the capsized catamaran on the final day of the simulation	Mean Lagrangian displacement (in m)	Standard deviation of mean Lagrangian displacement (in m)
200	87.51	135.28	9.99	0.02	0.01
500	91.16	186.40	25.49	0.02	0.02
1000	85.74	329.08	22.48	0.07	0.04
2000	76.69	357.94	26.74	0.06	0.04

Horizontal Eddy Diffusivity

To assess the impacts of stochastic motion on virtual particle trajectories along the southern coast of South Africa, experiments were derived based on the research carried out by Abernathey and Marshall (2013) and Rühs et al. (2018) who found an estimated range of surface horizontal eddy diffusivity for the Agulhas Bank of between 200 and 2000 $m^2.s^{-1}$. Therefore, four fixed values of horizontal eddy diffusivity were chosen for the estimation of the stochastic Brownian motion Hida (1980), notably 200, 500, 1000 and 2000 $m^2.s^{-1}$, as shown and compared in the following analysis (Table 4.1 and Figure 4.6). The percentage of virtual particles that hit the coast of South Africa were calculated to assess how different horizontal eddy diffusivities impacted the outcomes of the virtual particles. The relatively high values of particles reaching the coast in all of the experiments (>75 %) suggest that the dominant flow results from the surface currents and windage in a north-westerly direction which is pushing the virtual particles towards the coast. The experiment with the highest amount of diffusivity (2000 $m^2.s^{-1}$) had the lowest number of virtual particles hitting the coastline (76.69%). Furthermore, this experiment also resulted in the highest maximum distance from the recovery site of the capsized vessel (357.94 km). This is expected since the large horizontal eddy diffusivity results in stronger turbulence that, in turn, makes it less likely for particles to obtain comparable trajectories.

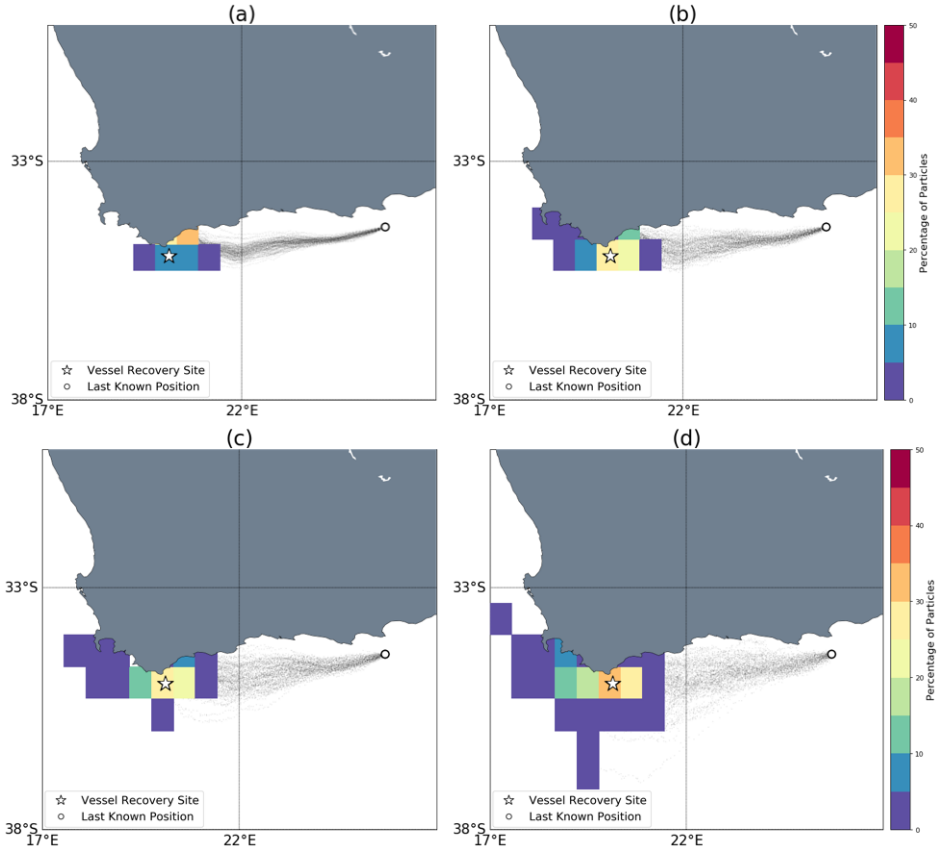

Figure 4.6: Illustration of the impact of the four different fixed horizontal eddy diffusivities on the outcome and pathways of the virtual particles. The fixed values of horizontal eddy diffusivity for each experiment is (a) 200, (b) 500, (c) 1000 and (d) 2000 $m^2.s^{-1}$. The $0.5^\circ \times 0.5^\circ$ bins represent the percentage of particles that fall within each bin between the final day of simulations (day 4 – 5). The grey lines indicate the trajectories of all 1000 particles for the duration of the experiment. The black and white circle represent the last known position of the capsized vessel and the black and white star represent the recovery site of the capsized vessel.

This is confirmed in the lower horizontal eddy diffusivity (200 and 500m^2s) simulations, where there is a greater percentage of virtual particles that reach the coast (87.51 % and 91.16 %) at a lower maximum distance from the recovery site (135.28 and 186.40 km respectively). This spatial feature, in accord with the non-turbulent pathways of particles, may be partly explained due to the lack of information associated with the statistical properties of fluctuating components of motion.

The tentative results of diffusion analysis suggest that the experiment with the lowest value of mean Lagrangian displacement (Mx) of 0.02 ± 0.01 was the experiment with the lowest horizontal eddy diffusivity, while the highest was 1000 $m^2.s^{-1}$ experiment with an Mx of 0.07 ± 0.04. The influence of the horizontal eddy diffusivity on the trajectory and final location of the virtual particles is presented in Figure 4.6. The overall direction of the virtual particles for all the experiments tends to be in a westward direction regardless of the value of horizontal eddy diffusivity. The horizontal eddy diffusivity influences the directional spread of the virtual particles, with higher horizontal eddy diffusivity resulting in greater variability and vice versa. To better quantify this variability, the percentage of total virtual particles in the ocean per $0.5^\circ \times 0.5^\circ$ grid at the end of day 5 is calculated. This provides an estimate of the maximum likelihood for a virtual particle to be found in a $0.5^\circ \times 0.5^\circ$ geographical grid on the last day of the simulation experiment.

As shown in Figure 4.6 the highest percentage of virtual particles on the day when the capsized vessel was recovered (day 4-5) are found in the 0.5° grid cell that contains the location where the capsized catamaran was recovered in three of the simulation experiments (Figures 4.6 b, c, d). The results suggest that the lowest fixed horizontal eddy diffusivity ($200m^2s^{-1}$) based on the studies by Abernathey and Marshall (2013) and Rühs et al. (2018), may be too low for this highly dynamic region. A relatively low 10 % of virtual particles that were deployed in this experiment made it to the bin where the capsized vessel was located. In the other three experiments, however, this percentage encouragingly exceeded 20 %. The experiments used a fixed diffusivity and did not account for the spatial variability of diffusivity fields, which will have an impact on the results and will be addressed in a future study.

Virtual Particle Forcings

To assess the importance of including both wind and surface current data when conducting simulations on capsized vessels in the ocean, experiments were conducted to assess the contribution of each forcing field (Figure 4.7).

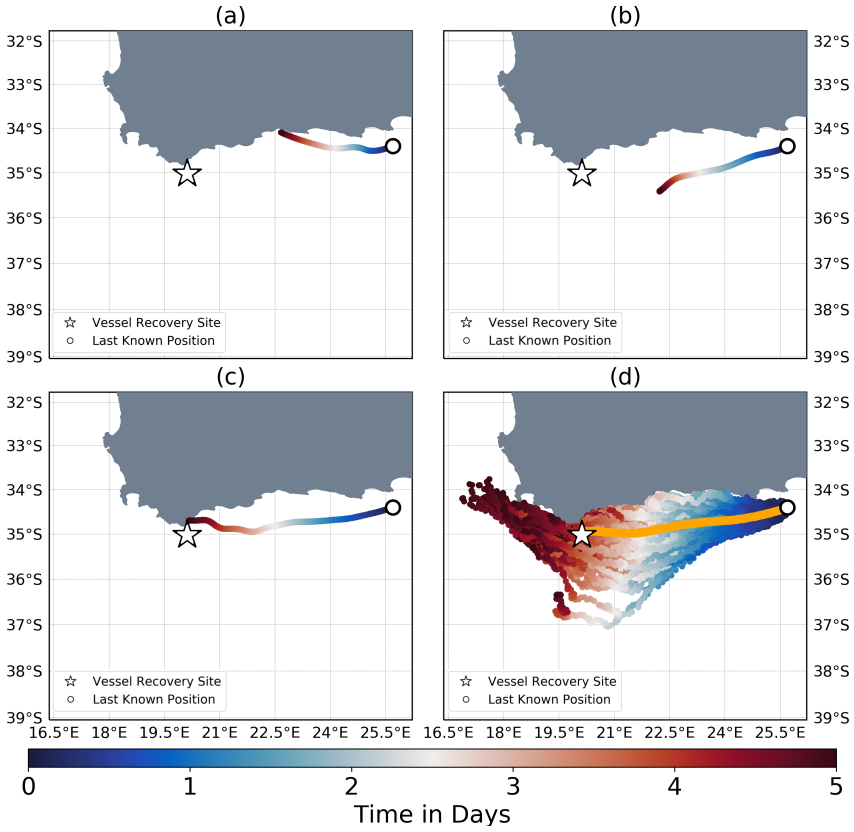

Figure 4.7: A simulation of 1000 virtual particles deployed at the location where the capsized vessel was last seen (white circle) forced (a) wind only, (b) current only, (c) wind and current only and (d) wind, current and Brownian motion. The colorbar represents the time in days since deployment, reaching a maximum of five days. The orange line on (d) represents the mean trajectory of the 1000 particles. It should be noted that (c) hits the coast after 4.1 days of the simulation.

The virtual particles in simulations forced with only surface currents (Figure 4.7b) are in agreement with Hart-Davis et al. (2018b) who suggest that using only ocean surface currents to force the synthetic particles is inadequate in terms of simulating the pathway of the capsized vessel. Although surface current velocity data plays a key role, this result suggests that other parameters play important roles in determining the accuracy of the trajectory of a capsized catamaran. Wind forcing only was also not sufficient (Figure 4.7a) and, although combining wind and surface currents (Figure 4.7c) improved the result significantly, the results remained insufficient in estimating the path of the capsized vessel.

This could be due to the spatial resolutions of the surface current velocity data (1/12°) and the wind data (1/10°) which are not able to represent the correct effects of unresolved processes of the region.

The resolved scales are provided from the ocean circulation model through the eddy diffusivity, which contributes to the stochastic forcing of the particle trajectory model. In an attempt to parameterise the unresolved processes in the particle trajectory model, Brownian motion (Hida, 1980) was applied to account for the turbulent features not resolved in the velocity field (Figure 4.7). The results show a strong number of virtual particles that pass through the point where the capsized vessel was recovered. When combining this result with the results shown in Figure 4.6, it can be implied that the particle trajectory model performs the best when the wind, surface currents and stochastic motion are incorporated as a high percentage of virtual particles end up in the region where the capsized vessel was recovered at the end of the simulation.

4.2 Comparison of Drifter Pairs

4.2.1 Drifter Observations

To further understand the impact of small scale processes on lateral transport of objects at the ocean surface, the trajectory of two drifters deployed in the Agulhas Current is assessed in this section. On the 11th of April 2015 at 16:45, two drifters (drifter 14901 and drifter 14547) that were provided by the South African Weather Service were deployed from the RV Algoa in the core of the Agulhas Current at 33,9034°S and 27,753°E as part of ASCA and SAGE activities (Morris et al., 2015). Remarkably, these two drifters, after being deployed at the same location, remained in close proximity to each other through their pathways in the Agulhas Current, the Agulhas Retroflection and the Agulhas Return Current. Only in the vicinity of the Agulhas Plateau did the two drifters separate.

To enhance insights on environmental conditions throughout the drifters' pathways in the Agulhas Current, the weekly-mean SST fields, calculated from the Global 1km Sea Surface Temperature (G1SST) Level 4 dataset (Ocean, 2010), are compared to the drifter trajectories (Figure 4.8). The SST fields, with drifter tracks overlaid, show that the drifter pathways tend to follow the shape of the current quite well. The trajectories of drifters in the Agulhas Current core tend to converge to regions of higher velocities (Hart-Davis et al., 2018b) explaining why there is little separation between the two drifters in week one. When the drifters reach the Agulhas Retroflection (week two), the shape of the current (as seen in Figure 4.8) shows very little variation resulting in the drifters following similar trajectories. In week three, the drifters begin to show slight variations, with drifter 14901 beginning to fall behind drifter 14547 but the drifters still follow the same pathways of the current. This slight variation between the two drifters could be a result of the meanders of the current before the Agulhas Plateau which is known to cause extreme levels of mesoscale variability (Lutjeharms and Ansorge, 2001). In week four, drifter 14547 follows the U-shape of the current remarkably well, however, this is where drifter 14901 begins to deviate from both the dominant current path and from drifter 14547.

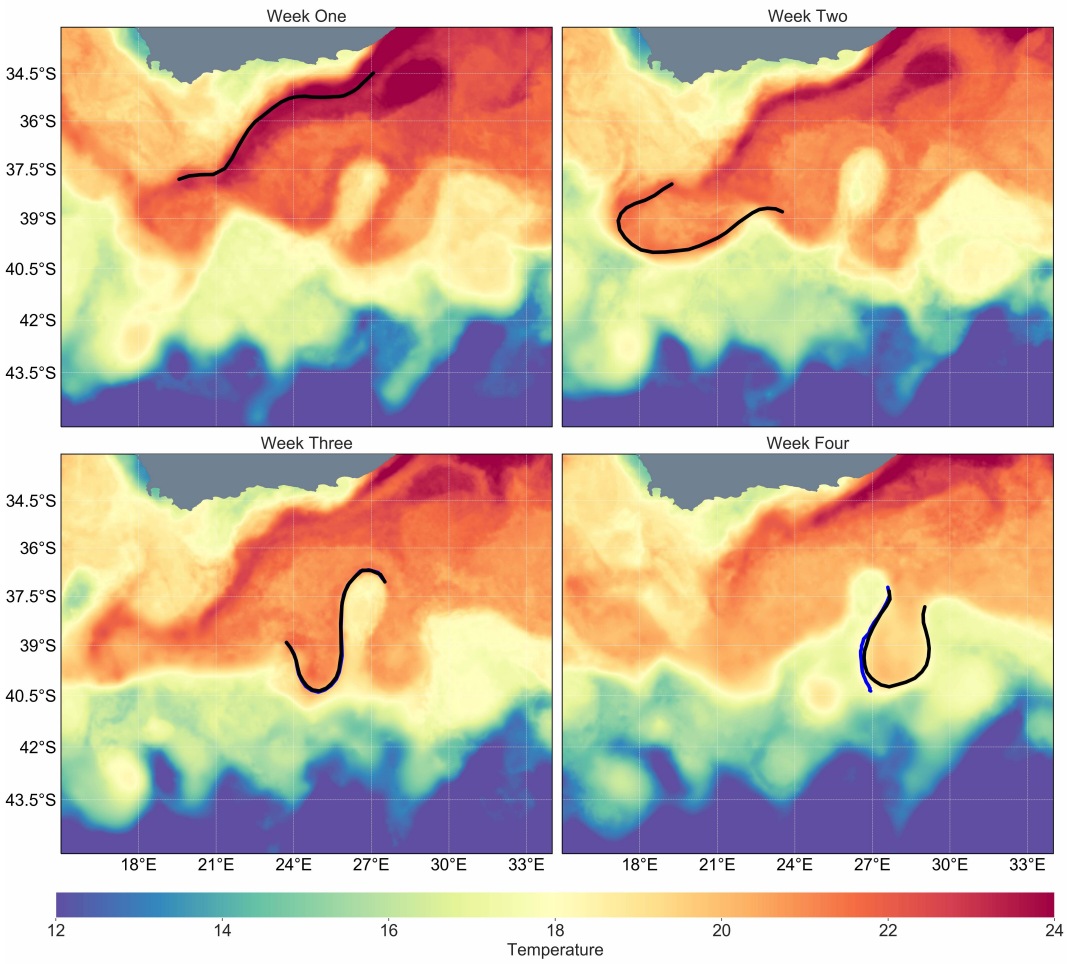

Figure 4.8: The drifter trajectories overlaid onto sea surface temperature (°C) fields extracted from the satellite derived G1SST Level 4 dataset (Ocean, 2010) for the first four weeks of the drifters lifespan. Drifter 14901 is represented by the blue line (only really visible during week four due to matching trajectories) and drifter 14547 by the black line.

The formation of an eddy on the Agulhas Plateau and at around 25°E and 40.5°S influences the variability of the region and invokes a change in the pathway of drifter 14901 from drifter 14547. Eddies in this region are well-documented (Lutjeharms and Valentine, 1988, Lutjeharms, 2006) although their impact on the meso and submesoscale variability of the region remains unclear (Backeberg et al., 2008).

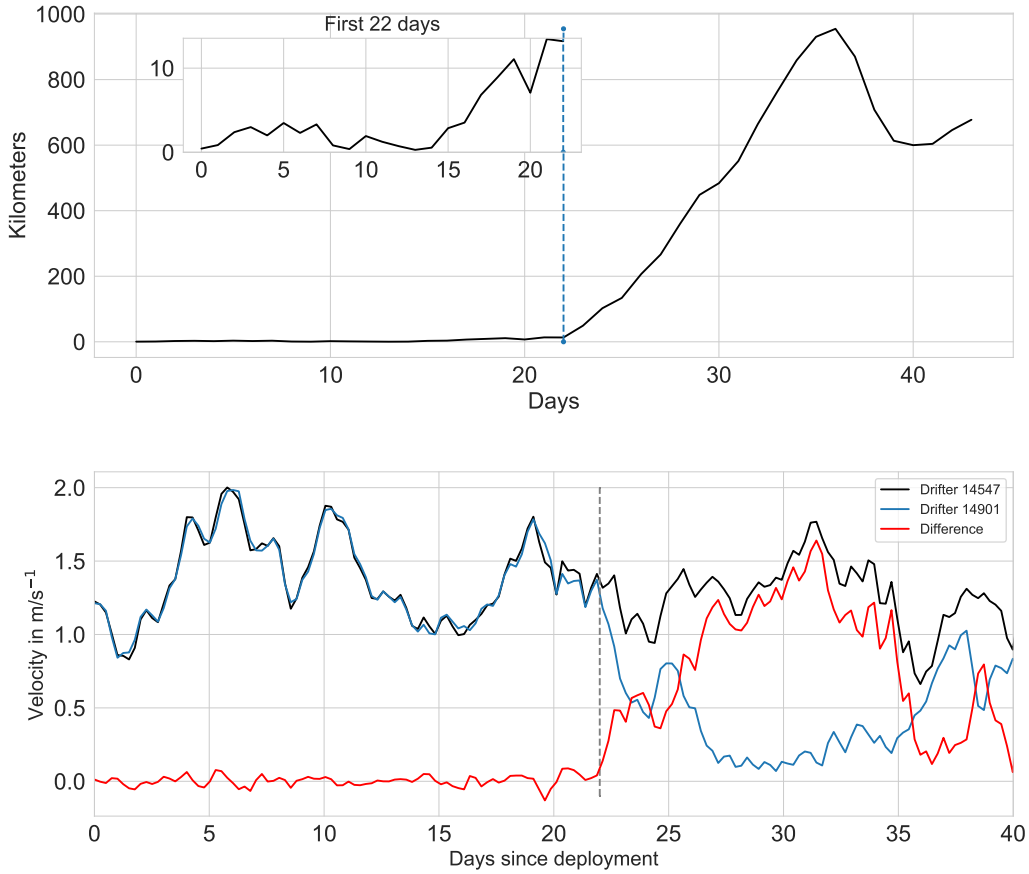

Figure 4.9: Distance separation (in km) between drifter 14901 and drifter 14547 over time. The blue dotted line indicates day 22 which is the point after which the separation grows almost exponentially. The sub-figure illustrates the distance separation for the first 22 days. The velocity ($m.s^{-1}$) of drifter 14547 (blue) and drifter 14901 (red) for the first 40 days (bottom). The grey dotted line indicates the 22nd day and the black line represents the difference in velocity between the drifters.

When considering the meanders and apparent formation of these eddies, it is assumed that the drifters are experiencing significant mesoscale variability (Lutjeharms and Valentine, 1988). A time series of the drifter separation is shown in Figure 4.9. On day 22 (week 4), a drastic increase in the separation between the drifters is encountered, suggesting that the drifters were suddenly exposed to different dynamical conditions. This separation increases almost exponentially for the remainder of the drifters' lifespans.

To further examine and understand the trajectories of this drifter pair, the velocity and vorticity of the drifters were calculated along their lifespan (Figure 4.9 and Figure A.4 of Appendix A). As expected, the drifter velocities remain high and similar throughout the first 20 days of their lifespan, which documents the minor drifter separation. On the other hand, on day 22, an increase in velocity difference, as well as a spike in vorticity, can be seen. This demonstrates that the pathway of drifter 14901 is less influenced by the strong Agulhas Return Current and more strongly influenced by the meso and submesoscale activity that is occurring in this region. The distance between the drifters on day 22 was 7.78 km, indicating that a submesoscale length process (1 km to 10 km in size; (Trotta et al., 2017)) is occurring in this region and having an impact on the drifter pathways. It is from this point onwards that the drifters' pathways begin to differ for the rest of their lifespans. In order to understand what processes may be affecting the drifter trajectories, surface ocean current products are introduced into the study.

4.2.2 Surface Ocean Product Analysis

The GlobCurrent (3-hourly) and the CMEMS 15 m ocean current velocities were extracted at the drifter locations and drifter dates to compare with the drifter velocities (Figure 4.10). Generally, the GlobCurrent ocean current velocities and the drifter velocities show an agreement in terms of shape, except for some periods where the GlobCurrent velocities tend to underestimate the velocities of the drifter. This is consistent with the study reported by Hart-Davis et al. (2018b) which found that, in the Agulhas Current, GlobCurrent underestimated the velocity of drifters by about 27 %. The mean velocities calculated from GlobCurrent and CMEMS underestimates the mean velocity of the trajectory of drifter 14901 by 14.19 % and 19.27 % respectively. The underestimation is even greater for drifter 14547, with the GlobCurrent velocities underestimating the mean drifter velocity by 25.10 % and CMEMS, 41.84 %.

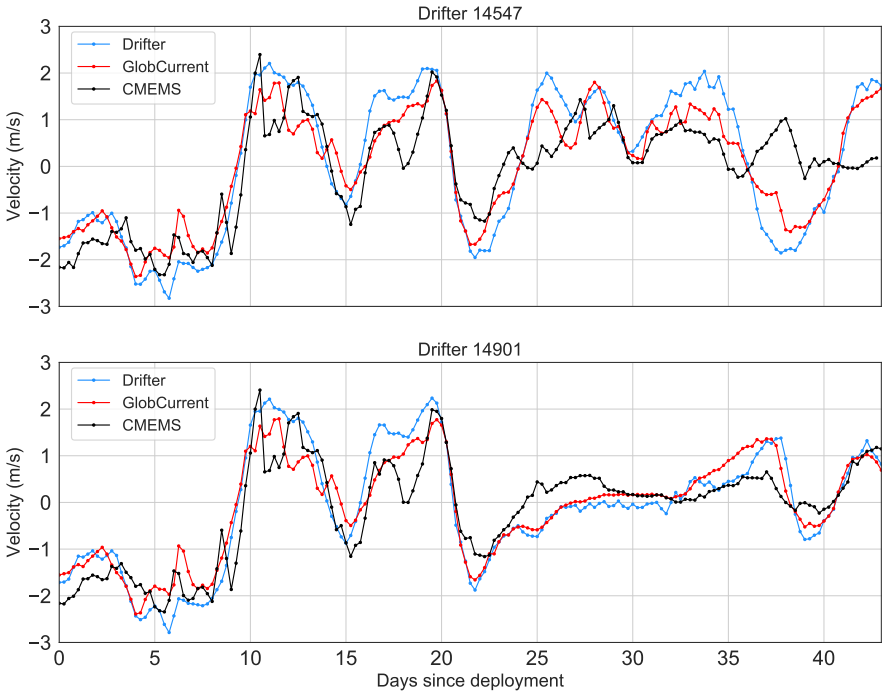

Figure 4.10: At each position of the drifter trajectories, the GlobCurrent (red) and CMEMS (blue) velocities were extracted to compare against the velocities of the drifters (black).

The CMEMS product tends to vary considerably from the velocity profile of the drifters, in some regions exceeding the drifter velocities (within the first three days) while in some periods the velocities are shown to go in opposite directions. To characterize the consistency between both drifters and the GlobCurrent and CMEMS products with quantitative metrics, the skill scores were computed (Figure 4.11) based on the methodology proposed by Liu et al. (2011) and used by Cancet et al. (2019) to assess GlobCurrent in the East Australian Current. This non-dimensional skill indicates the relative performance of the products compared to the drifter observations (Cancet et al., 2019) and, therefore, allows for the comparison between the two ocean products in representing the dynamic processes and variability encountered by the two drifters in the different regions of the Agulhas Current system.

For each position of the two surface drifters, the trajectories of the virtual drifters were estimated using both the GlobCurrent and CMEMS ocean products. Instead of using one virtual drifter, an ensemble average of ten virtual drifters were used to compensate for the horizontal diffusivity. The virtual drifters were deployed for 3-days with a sampling frequency of six hours to align with the surface drifters.

The skill score as formulated by (Liu et al., 2011) is written as follows:

$$\begin{aligned} s &= 1 - c(c \leq 1) \\ s &= 0(c > 1) \end{aligned} \tag{4.1}$$

where,

$$c = \frac{\sum_{i=1}^{N} d_i}{\sum_{k=1}^{M} l_k}. \tag{4.2}$$

For each point on the surface drifter trajectory, N represents the number of virtual drifter dates during the 3-day period, while M is the number of drifter dates during the same period. For both cases, N and M were always equal ($N = M = 12$) as the virtual drifters were deployed with the same sampling frequency as the surface drifters. c is the cumulative Lagrangian separation distance (d) divided by the cumulative length of the observed trajectory (l) (Cancet et al., 2019). When $c > 1$, the cumulative separation of the virtual drifters is larger than the cumulative length of the observed trajectory. When $s = 1$, the virtual drifters are perfectly matching the drifter trajectories. Figure 4.11 and 4.12 and Table 4.2, illustrate the skill scores during a 40-day period for both drifters using the GlobCurrent and CMEMS product respectively. It is expected that due to the highly varying sub-meso and mesoscale variability of the Agulhas Current System, the abilities of the ocean products will vary dependent on the region the drifters are passing through. The fast flowing nature of the Agulhas Current, known to exceed $2m.s^{-1}$ (Rouault et al., 2010), implies that the Lagrangian separation of the surface drifters will be relatively high and due to the underestimation of the surface ocean currents by the ocean products, seen in Figure 4.10 and shown in Hart-Davis et al. (2018b), it can be expected that the skill scores will be greatly affected in this region.

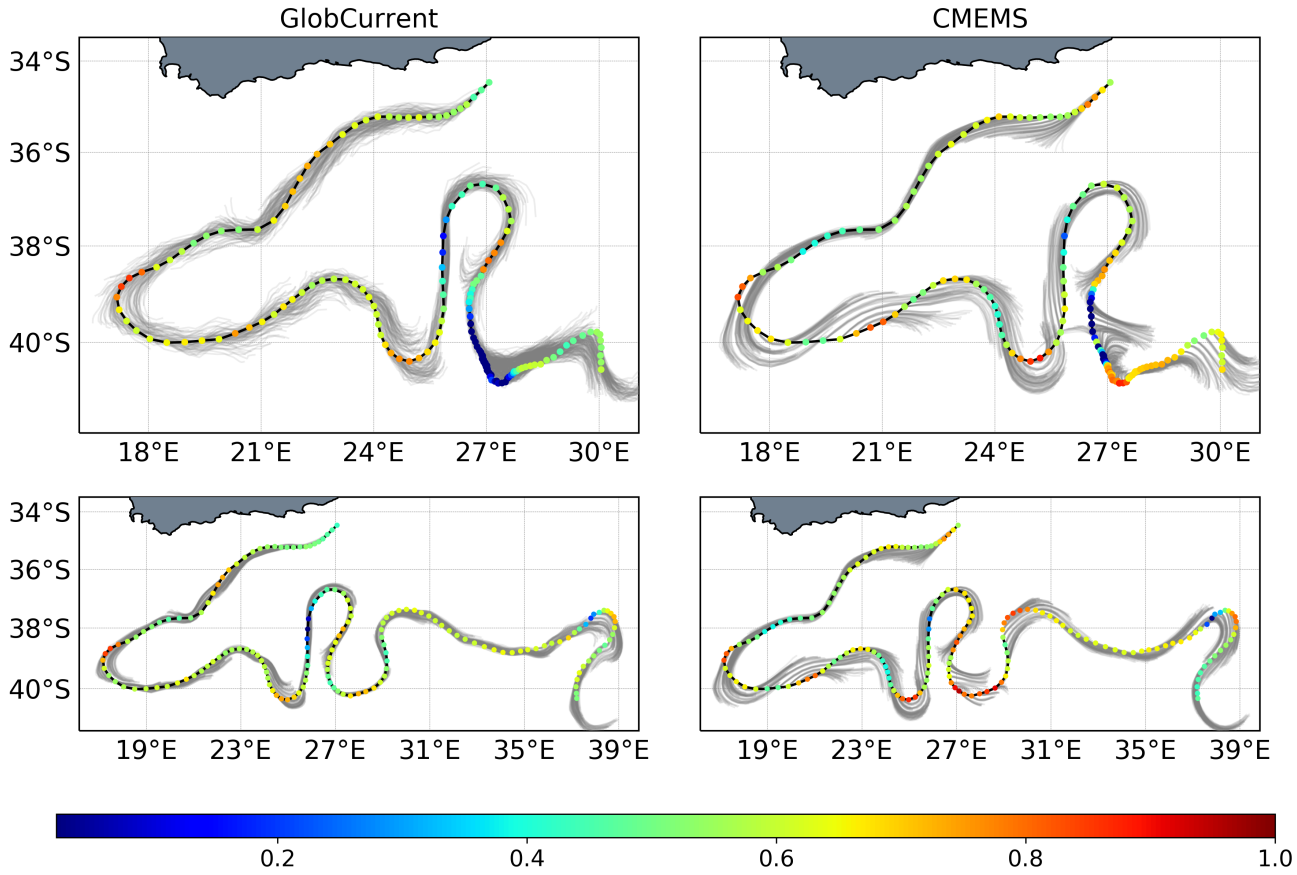

Figure 4.11: Skill scores after three days of advection with 3-hourly total 15m GlobCurrent current velocities and 15m CMEMS current velocities. The light gray lines show the trajectory of ten virtual drifters deployed at each position of the drifter trajectories and after three days of advection by the respective ocean product.

In the Agulhas Current, the overall shapes represented by the virtual drifters agree well with the surface drifter trajectories for both products, particularly in the GlobCurrent product. Furthermore, both products have similar skill scores in this region. This similarity is further shown in Figure 4.12 where initially the skill score of CMEMS is higher but further along the trajectory GlobCurrent shows higher scores. Despite the underestimation of the surface currents, the skill score in this region is still relatively good suggesting that the two ocean products satisfactorily represent the Agulhas Current. Furthermore, in the Agulhas Retroflection, the shape of the virtual drifter trajectories do a good job in representing the expected flow shape of the current.

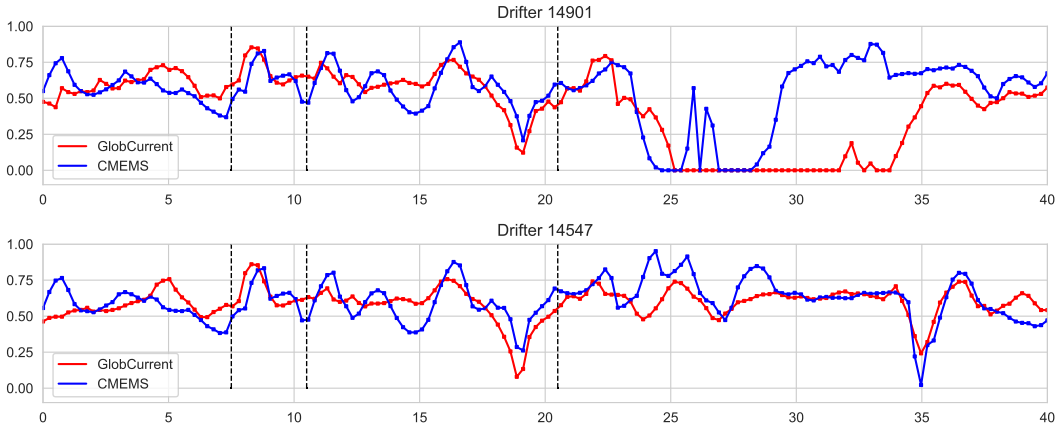

Figure 4.12: Time series of the skill scores along both drifter trajectories for GlobCurrent velocities (red) and CMEMS velocities (blue). The black dotted vertical lines show the sub-regions (the Agulhas Current, the Agulhas Retroflection, before Agulhas Plateau Meander and after Agulhas Plateau meander) that are discussed in the text.

Table 4.2: The average skill score in each of the experiments in the different sub-regions.

Sub-region	GlobCurrent D14547	GlobCurrent D14901	CMEMS D14547	CMEMS D14901
Total	0.439	0.593	0.549	0.610
Agulhas Current	0.587	0.572	0.567	0.570
Agulhas Retroflection	0.689	0.669	0.639	0.637
Before Meander	0.565	0.559	0.573	0.580
After Meander	0.279	0.607	0.517	0.637

Cancet et al. (2019) presented satisfactory skill scores (between 0.6 and 0.9) for GlobCurrent virtual drifters in large-eddy structures, and this is further demonstrated for GlobCurrent in the Agulhas Retroflection with the mean skill score being 0.664, with the values reaching as high as 0.860. In comparison, the CMEMS virtual drifters perform relatively well in this region as well, showing a mean skill score of 0.638. Based on the spatial resolution of GlobCurrent and CMEMS, it is expected that the large scale Agulhas Retroflection would be well resolved by these two products.

For a more detailed comparison, the remaining trajectory of the drifters along the Agulhas Return Current is divided into two sections, before the Agulhas Plateau meander (up to 27°E and 36.7°S) and after the Agulhas Plateau meander (after 27°E and 36.7°S). This is designed to assess the ability of the products during the time of the strong separation of the two drifters. Before the meander, the shape of the GlobCurrent forced virtual drifters again agree well with that of the surface drifters with the only major difference happening at the meander that occurs before the Agulhas Plateau meander (at approximately 25°E). The trajectory of CMEMS forced virtual drifters also matches the expected shape of the current, but there seems to be a greater deviation from the observed surface drifter trajectories, particularly directly after the Retroflection and in the meander before the Agulhas Plateau meander.

In terms of skill score (Table 4.2), the GlobCurrent virtual drifter performs relatively consistently at ±0.6, while the skill scores of CMEMS virtual drifters are rather inconsistent during the period directly after the meander. However, both ocean products show a relatively drastic drop in terms of the skill score before the Agulhas Plateau meander (at around day 18). During this period, the current is flowing relatively fast, at some points exceeding $2m.s^{-1}$, and both ocean products are underestimating the velocity of the surface drifters (Figure 4.10). Even though the virtual drifters are following a similar shape to that of the surface drifters, the underestimation in terms of velocity simply force the virtual drifters to travel a shorter distance. This explains why the skill scores (due to the lower Lagrangian separation) suggest a poor performance of both ocean products in representing the expected dynamics experienced by the drifters during this period.

The meanders of the Agulhas Return Current are also characterized by having strong mesoscale variability (Lutjeharms and Ansorge, 2001) while the Agulhas Plateau is known for its recurrent eddy generation (Lutjeharms and Van Ballegooyen, 1988). This variability provides a further explanation for the relatively low skill scores as well as the velocity underestimation of both ocean products in this region. As the surface drifters meander around the Agulhas Plateau both ocean products perform satisfactorily initially, but this is when the performance of the ocean products becomes different for each surface drifter. The satisfactory initial skill scores around the meander is encouraging as this is where the major separation occurs between the two drifters.

Furthermore, the low skill scores thereafter (between day 23 and 24) indicates that the processes affecting the drifters are not being represented by both ocean products. After day 25, both ocean products perform poorly for drifter 14901. The poor performance of both ocean products in this region is largely due to both products not being able to properly capture sub-mesoscale variability in this region which influences the trajectories of the two observed surface drifters. However, of the two products in this part of the study, the CMEMS ocean product performs the best, which is likely due to its higher spatial resolution. The trajectory of the virtual drifters for both ocean products are shown to be affected by the Agulhas Plateau eddy as some continue to move in the clockwise direction instead of flowing south. This suggests that the dominant current is relatively weak, which can be seen in the velocity of the drifters from day 22 to day 30 (Figure 4.10), and, therefore, the eddy is having an influence on the mesoscale variability in the region. When assessing the SST fields in Figure 4.8, it was previously suggested that this eddy could be a reason for the deviation between the two surface drifters. As the influence of these processes can be seen in both surface current products and the SST product, it can then be implied that the separation between the two surface drifters was largely due to the sub-meso and meso-scale variability introduced by the formation of the Agulhas Plateau eddy and the weakening of the current.

4.3 Early life dispersion of juvenile loggerhead turtles

Section 4.2 highlighted how Lagrangian particle trajectories can be used to study how passive objects (drifters) can move from the ocean. Similar methods can be used to be applied to study the movement of passive drifting marine organisms. Additionally, virtual particles can be given swimming characteristics to simulate how active swimmers move in the ocean. The dispersion of marine organisms, particularly larvae, is mainly driven by the ocean currents and several studies have used passive virtual particles to study their drift and trajectories (e.g. Singh et al. (2018)). However, when studying the biological connectivity of certain marine organisms, their behaviour needs to be taken into account to give a proper representation of their movement (Van Sebille et al., 2018). For instance, very little is known about the movement patterns of sea turtles both in terms of horizontal and vertical migration (Freitas et al., 2019).

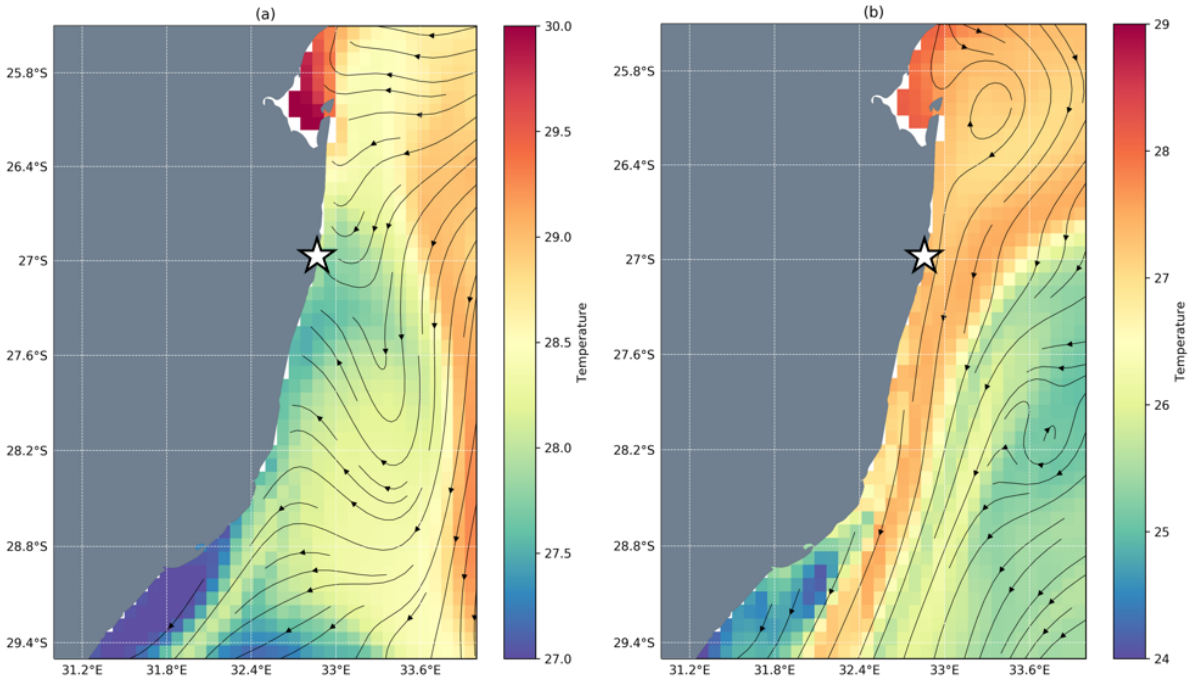

Figure 4.13: An illustration of the surface current velocities and sea surface temperatures (°C) around Beacon 4N (represented by the white star) as represented by the CMEMS ocean product for 2017 (a) and 2018 (b).

As mentioned in Section 2.5, a study by Bolten (2003a) modelled the dispersal patterns of South African juvenile turtles under the assumption that they had passive drift. However, the proposed life history of juvenile loggerhead turtles suggests that after they swim away from their hatching site, they spend more than a decade in the oceanic environment passively drifting in the ocean currents and only (Bolten, 2003a).

Hence when using particle trajectory modelling to study the fate of hatchling sea turtles, the swimming characteristics of the turtle needs to be included to give a proper representation of their oceanic spatial distribution and ecology. To investigate this within Parcels, an experiment was conducted to test the impact of initial swim speed on the resultant trajectory of loggerhead turtle hatchlings (Chapter 2.5). Three separate scenarios over two years were run at the known hatching site of loggerhead turtles on the east coast of South Africa (26.9960°S and 32.8658°E).

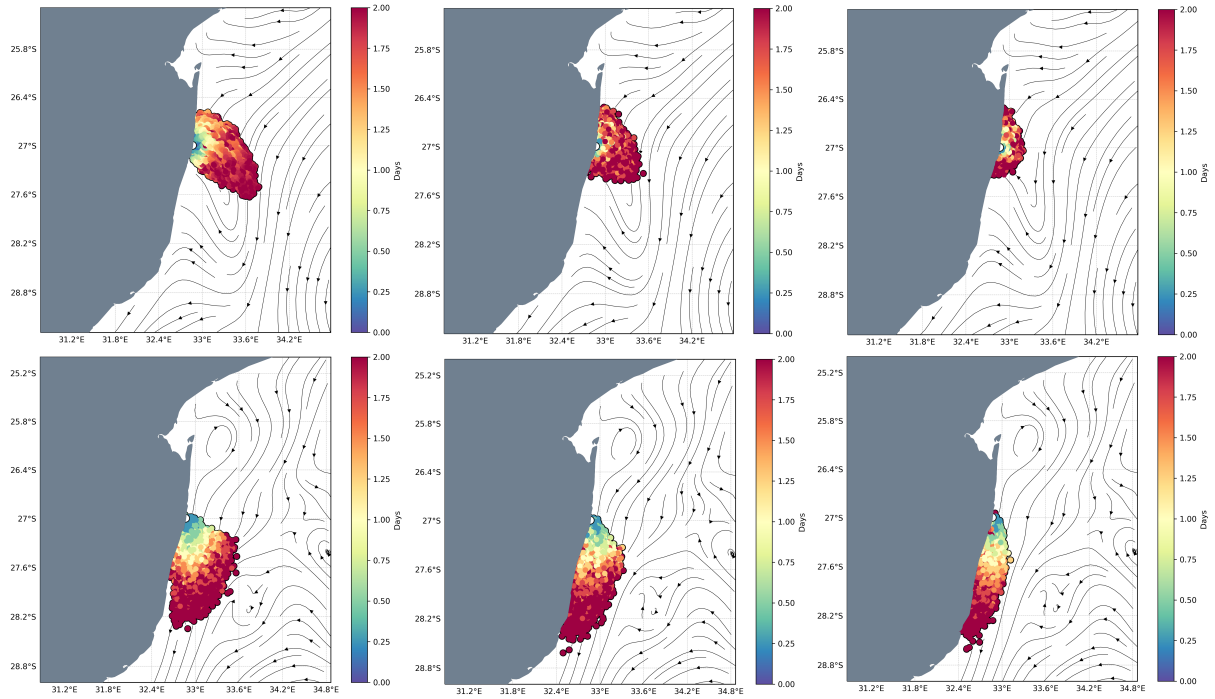

Figure 4.14: An illustration of the first two days of the virtual turtles life for each of the three scenarios for both 2017 and 2018 overlaid onto streamlines of the surface current velocities from the CMEMS ocean product. The top row is the 2017 scenarios and the bottom row is the 2018 scenarios. From left to right in each column: trajectories with 1.0 $m.s^{-1}$ swim speed, with 0.5 $m.s^{-1}$ swim speed and with no swimming. The colorbar represents the time in days since deployment of the virtual turtles.

The virtual 'turtles' were given three separate initial conditions: (a) $1.0m.s^{-1}$ to represent the expected maximum real velocity of the juvenile loggerheads; (b) $0.5m.s^{-1}$ to represent the average expected velocity of the juvenile loggerheads and (c) passive particles to represent no swimming. The input ocean surface velocity data used to run the virtual turtles for all experiments was the CMEMS ocean product (Chapter 3.2.3) with the 'dead zone' boundary condition was used (Chapter 3.3.2). Figure 4.13 shows the surface current velocities overlaid onto the sea surface temperature. For each scenario, 15,000 virtual turtles were deployed for 100 days on the 15th of February (representing the peak hatchling time) over two years, 2017 and 2018, to incorporate the strong inter-annual oceanographic variability at the nesting site, with the separate initial swimming conditions. It can be seen that the inter-annual dynamics of the region varies considerably in 2017 and 2018.

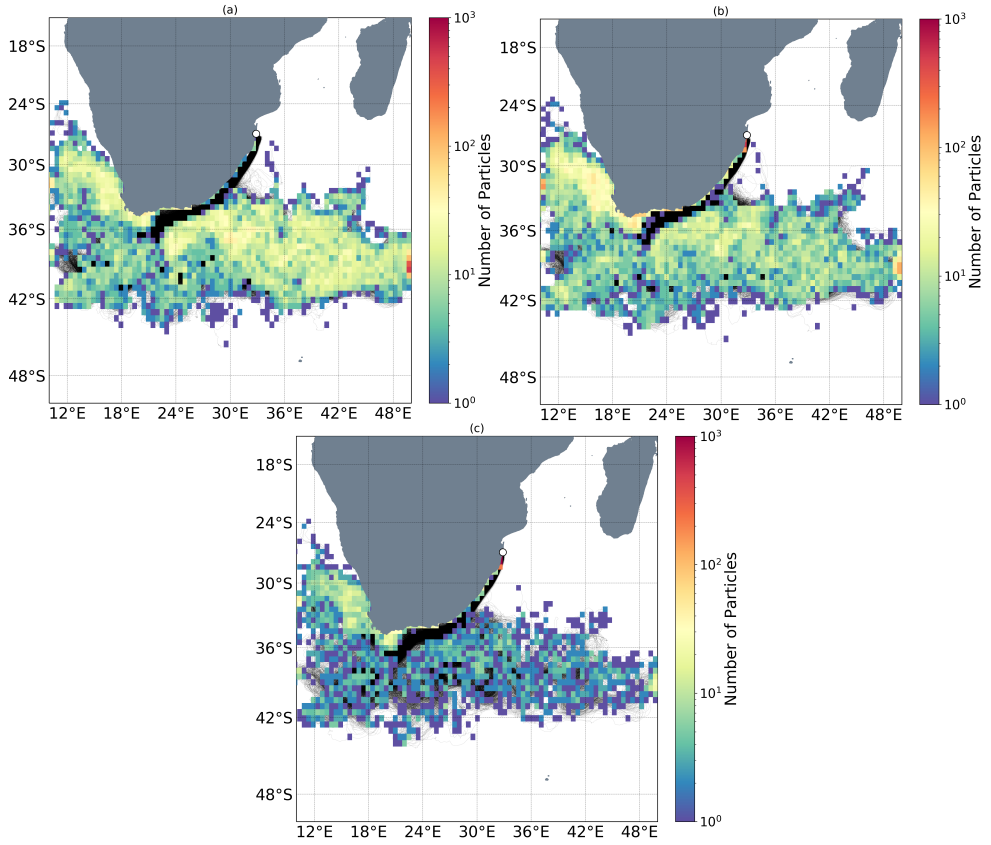

Figure 4.15: Density plots for the final position and full lifespan trajectories (black lines) of virtual turtles for each scenario in 2018. The trajectories of turtles (a) with 1.0 $m.s^{-1}$ swim speed, (b) with 0.5 $m.s^{-1}$ swim speed and (c) with no swimming.

This will have an impact on where the turtles end up and, therefore, provide a suitable test for the impacts of swimming on the resultant trajectories of virtual turtles. For every scenario, the trajectory of the virtual turtles will be assessed to evaluate where they end up within the ocean or if they become stranded along the coast of southern Africa. Results of the simulations reveal that swimming has an impact on the resultant trajectories of the virtual turtles (Figure 4.14, 4.15 and 4.16). It can be visually seen in the density plots that more virtual turtles make their way down the coast of South Africa, particularly in the simulations run for 2017. As seen in Figure 4.15 of 2017, the currents are landward at the point where the virtual turtles are being deployed.

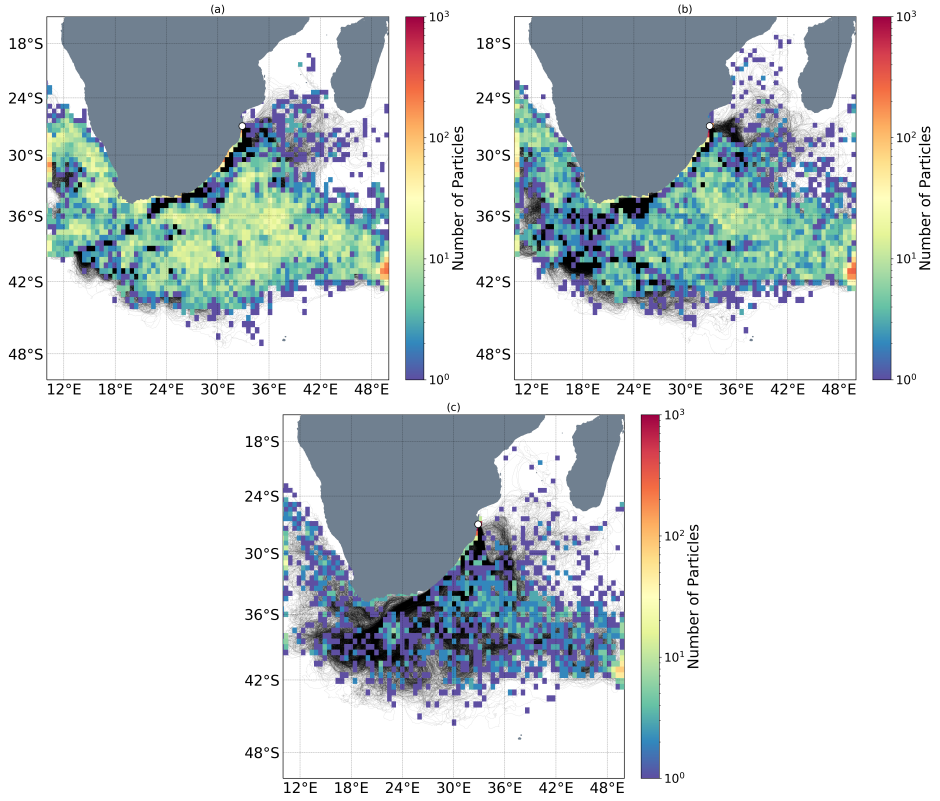

Figure 4.16: Density plots for the final position and full lifespan trajectories (black lines) of virtual turtles for each scenario in 2017. The trajectories of turtles (a) with 1.0 $m.s^{-1}$ swim speed, (b) with 0.5 $m.s^{-1}$ swim speed and (c) with no swimming.

This means in the scenario where no swimming is added to the virtual turtles, a large majority of the virtual turtles are pushed onto land and hit the boundary very soon after deployment (as seen in Table 4.3 and 4.4). In fact, 64.26 % of the virtual turtles deployed hit the land within 10 km of the deployment site. When applying swimming speed, this percentage decreases to 12.04 % with half swim speed and 0.30 % with the full swim speed. Looking at the 2018 scenario, considerably less virtual turtles with no swim speed hit the land close to the deployment site (28.33 %) which is mainly due to the dominant current being parallel to the coast at the time of deployment, hence there is less of a landward push of virtual turtles. When applying the swim speed this decreases even further with only 2.95 % and 0.07 % (only one) of the virtual turtles hitting the land for half swim speed and full swim speed scenarios respectively.

Table 4.3: The percentage of the 14,884 virtual turtles deployed for 100 days for each scenario that reach a region of interest (a).

Scenario	Turtles Deployed	Turtles that hit land	Hit Land Close to Hatch Site	Benguela Current	Agulhas Current
2017 a	14,884	74.46	0.30	1.81	13.11
2017 b	14,884	78.92	12.04	1.28	29.00
2017 c	14,884	93.89	64.26	0.25	23.17
2018 a	14,884	16.27	0.07	12.17	7.16
2018 b	14,884	71.55	2.95	19.86	22.34
2018 c	14,884	78.80	28.33	6.81	49.32

Table 4.4: The percentage of the 14,884 virtual turtles deployed for 100 days for each scenario that reach a region of interest (b).

Scenario	Agulhas Return Current	Agulhas Retroflection	South-East Atlantic Ocean	Agulhas Recirculation	Indian Ocean
2017 a	29.76	1.92	21.81	29.52	1.93
2017 b	20.44	1.85	14.71	21.69	1.97
2017 c	5.16	0.44	2.91	6.21	0.52
2018 a	11.39	6.54	7.26	55.42	0.01
2018 b	7.69	7.46	9.80	31.66	0.00
2018 c	1.99	2.73	2.99	7.64	0.00

These findings illustrate the importance of including the initial swim speed on getting virtual turtles away from the deployment site. If an experiment was conducted studying the pathways of turtles in 2017 using no swimming, the results would be skewed as only 355 virtual turtles would make it away from the deployment site. Table 4.3 and 4.4 reinforces this statement when looking at the final positions of the virtual turtles.

More virtual turtles end up in the Agulhas Return Current and the Benguela Current for both the swimming scenarios. This illustrates an important reason swimming behaviour of marine organisms needs to be considered when conducting connectivity studies or when trying to assess their movement behaviour. For instance, it is thought that the turtles that end up in the Benguela Current, where the temperatures are relatively low, have a lower survival probability than those that end up elsewhere in the Agulhas system.

If only the final locations of the passive virtual turtles are considered, it appears only a small percentage of turtles end up in the Benguela (0.25 % and 6.81 % for 2017 and 2018 respectively). When including swimming, this percentage increases for both years and both swim speeds (up to 19.86%). The ocean surface currents play a vital role in the fate of juvenile turtles once they enter the ocean, however, it is shown that incorporating swimming characteristics when studying the fate of juvenile turtles is important in providing a more realistic estimation of their pathways.

5

Summary and Conclusion

The research presented in this thesis investigated the following hypothesis: *Lagrangian ocean analysis can be used to provide a better understanding of the physical mechanisms that drive the processes occurring in the Greater Agulhas System*. This thesis had four objectives that all combined to contribute to testing the hypothesis, these are summarized in the below subsections 5.1 - 5.4.

5.1 Lagrangian Ocean Analysis

The importance of Lagrangian parameterizations, horizontal eddy diffusivity calculations and different boundary conditions, were assessed to understand the developed optimal particle trajectory model for different applications. The results showed that by using model-derived horizontal eddy diffusivity, the trajectory of virtual drifters better represents the trajectory of the real drifter. This was due to the spatially and temporally varying horizontal eddy diffusivity accounting for the lateral and vertical mixing processes not resolved properly by the ocean model data. It was shown that the implementation of boundary conditions improved the representation of the real drifter trajectory by the virtual drifters. Furthermore, the reflective boundary condition proved to be the best of the boundary conditions in improving the accuracy of virtual drifter simulations for studies of ocean dynamics.

5.2 Search and Rescue

A particle trajectory model combining ocean surface currents, winds and stochastic motions was assessed for potential application in a search and rescue scenario for a capsized catamaran drifting past Cape Recife, South Africa. The surface current product used, CMEMS, includes the influence of geostrophic and Ekman currents. The use of geostrophic currents itself cannot cause virtual particles to move towards land but when combined with Ekman currents the virtual particles can move towards land (Onink et al., 2018). It is shown that, by incorporating wind and surface current data into the particle trajectory model, the model more accurately predicts the drift of the capsized vessel over a five-day period. Furthermore, by incorporating the impacts of stochastic motion into the model, the model provides a better probabilistic forecast of the outcome of the capsized vessel. It is anticipated that with some refinement (such as using spatially varying horizontal eddy diffusivity calculations) and the incorporation of other parameters (e.g. interactions between wind, current, wave and turbulence), the accuracy of the particle trajectory model will improve and result in the increased use of this model in scientific and operational applications.

5.3 Comparison of Drifter Pairs

In section 4.2, the trajectory of a pair of surface drifters in the Agulhas Current system is analysed by looking at the sea surface temperatures as well as the particle trajectory model.

The surface drifters remained in relatively close proximity to one another for twenty-two days, following the Agulhas Current, the Agulhas Retroflection and part of the Agulhas Return Current. The drifter-pair separated from each other during their meandering trajectory around the Agulhas Plateau. Using the G1SST sea surface temperature product and considering the drifter velocities during the time of separation, there appears to be a weakening in the current strength and the formation of eddies on and south of the Agulhas Plateau. The formation of these eddies combined with the weakening of the current would enhance eddy-current interactions which may explain the almost exponential increase in the separation of the surface drifters.

The use of virtual drifters forced using the GlobCurrent and CMEMS ocean products provided interesting results to support this statement. Both products performed relatively well in imitating the trajectory of the real surface drifters when they were in regions dominated by larger-scale features (the Agulhas Current core and the Agulhas Retroflection). In the regions where smaller structures appear to be present, both products perform significantly worse, largely due to their underestimation of the drifter velocities. This suggests that the spatial and temporal resolution of the ocean products are too coarse to properly capture the sub-mesoscale dynamics of the region.

During the time where the separation occurs between the surface drifters, the virtual drifters of both products are shown to be influenced by the Agulhas Plateau eddy. It is, therefore, suggested that the eddy on the Agulhas Plateau and the weakening of the current velocity caused a regional enhancement of eddy-current interactions. This increased sub-mesoscale variability, not captured in the surface ocean products, facilitated the separation of the surface drifter-pair as they passed through this region. Following this, both surface drifters are exposed to different physical processes which result in the almost exponential separation between the drifter-pair.

5.4 Early life dispersion of juvenile loggerhead turtles

In reality, tracking juvenile turtles is an extremely difficult task as they are too small to carry the weight of GPS devices and cannot be followed with the naked eye for long periods. It is, however, important to understand the movement behaviour of these threatened turtles for legislative and conservation purposes. The introduction of new and innovative techniques such as the one presented in this thesis allows for the increased understanding of the geographical distribution of juvenile turtles.

The results of the study presented in section 4.3 emphasize the importance of including swimming behaviour when modelling the trajectories of juvenile turtles in the ocean and highlight the need to improve our knowledge of this life stage of sea turtle life history. As demonstrated, simply including the initial swimming behaviour of the juvenile turtles has a significant impact on where they end up 100 days later.

An important conclusion from this work is the necessary inclusion of the swimming behaviour to develop a better understanding of their geographical distribution and as a result, estimating the survival rate of these juveniles. Doing so will have implications for identifying areas where fisheries bycatch can cause enhanced mortality rates in juvenile turtles. Therefore, a better understanding of where juvenile hatchlings are likely to end up has implications for conservation measures put in place to protect the turtles.

5.5 Concluding Remarks

This thesis builds on the research done by Hart-Davis et al. (2018b) and presents the first attempt at developing a cross-disciplinary particle trajectory model for the Greater Agulhas System. In this thesis, a particle trajectory model is used in a search and rescue scenario, studies of ocean dynamics and studying juvenile turtle dispersion. The combined results of this thesis, confirm that Lagrangian ocean analysis can be used to provide a better understanding of the physical mechanisms driving processes occurring in the Greater Agulhas System.

With the refinements of Lagrangian parameters specifically for each of the experiments presented in this thesis, Lagrangian ocean analysis has provided valuable information for the better understanding of different processes being studied. Despite demonstrating that the particle trajectory model developed during this thesis is able to represent important processes in the Greater Agulhas System in a relatively accurate manner, several areas of improvement have been identified. Notably, the resolution of the ocean current and wind products used to force the particle trajectory model do not resolve the sub-grid scale processes that impact the trajectory of virtual particles in the ocean. Although this thesis adds horizontal eddy diffusivity to account for these turbulent motions, an improvement in spatial and temporal resolution of the input data forcing the virtual particles will allow for improved understanding of submesoscale processes. Therefore, future work could include using higher resolution numerical model ocean surface current and wind data to force the particle trajectory model. Furthermore, as mentioned in section 2.3, the trajectory of objects in the ocean is impacted by a variety of surface current components. Therefore, the particle trajectory model could be improved by incorporating these processes as well as by the improvement of spatial and temporal resolution of the numerical model data.

Finally, the applications of particle trajectory modelling developed during this thesis can be expanded to other applications to assist with the management of ocean-based operations. These applications could include, for example, incorporating the characteristics of other marine organisms' migration patterns, submesoscale ocean dynamics (using very high-resolution ocean and wind models), which in turn could assist with oil spill response management and studies of plastic dispersion.

With further refinement and development, particle trajectory modelling will provide a unique method to quantitatively study the oceanic processes and the distribution of objects in the ocean.

A

Appendix

Figure A.1: Summary of the specifications of Lagrangian Particle Tracking tools from Van Sebille et al. (2018)

Code name	Ariane	TRACMASS	Octopus	LAMTA	CMS	Parcels
Website	www.univ-brest.fr/lpo/ariane	tracmass.org	github.com/jinbow/Octopus	bitbucket.org/f_nencio/spasso/overview	github.com/beatrixparis/connectivity-modeling-system	oceanparcels.org
License	CeCILL (http://www.cecill.info)	open source	MIT	GNU General Public License	GNU GPL v3	MIT
Key citation	Blanke and Raynaud (1997); Blanke et al. (1999)	Döös et al. (2017)	Wang et al. (2016)	d'Ovidio et al. (2015)	Paris et al. (2013b)	Lange and van Sebille (2017)
OGCMs supported	NEMO/OPA, ROMS, Symphonie and any C-grid	NEMO, IFS (AGCM), MOM, MICOM, POM, HYCOM	MITgcm; any C-grid	AVISO satellite velocities; any velocity field on A-grids (euclidean or spherical)	HYCOM, OFES, NEMO, SOSE, MOM, MITgcm	NEMO, OFES, GlobCurrent; customizable to any OGCM with NetCDF data format
Language(s)	Fortran 90/95; Matlab (IDL on request) for visualisation	Fortran	Fortran	GNU/Octave and C++	Fortran	Python user interface, auto-generated C
Primary use	Offline calculation of 3D streamlines in the velocity field at any scale (regional, basin, global); volume transport calculations	3D water mass pathways, particle/tracer dispersion	3D watermass pathway, particle/tracer dispersion, cross-frontal transport, Argo float simulation	Compute satellite based Lagrangian diagnostics to optimize sampling strategy of mesoscale-based field campaign and support interpretation of in-situ observations	Dispersion, connectivity, fate of pollutants; Individual Based Modelling	Large scale oceanography; Individual Based Modelling; teaching (via customizable interface)
Advection method	Analytic	Analytic	RK4	RK4	RK4	RK4, RK45, Explicit Euler; extensible interface for custom advection methods
Diffusion method	No diffusion (purely kinematic method)	Brownian motion for background diffusion with random displacement or randomly added velocities	Brownian motion for background diffusion, random displacement within the mixed layer	Random walk optional	Brownian motion for background diffusion, random displacement within the mixed layer	Extensible interface for Random Walk and custom behaviour
Grids supported	Arakawa C, also tested with Arakawa B interpolated on C-grid, partial cells supported	Arakawa A, B, C. Spatially and temporally varying vertical grids supported (partial cells, z^*, sigma, hybrid) including those for AGCMs	Arakawa C	Arakawa A	Orthoknal (rectangular) Arakawa A, B and C	Arakawa A, B and C; unstructured meshes planned
Key strengths	Almost 25 years of experience with core of the code; easy-to-install, easy-to-use; fast analytical solution; no coast crash; qualitative mode (full details of selected trajectories) and quantitative mode (volume transport calculations); compatible with the conservation laws of the OGCM	Volume conserving, fast analytical solutions without intermediate time steps, works with both OGCMs and AGCMs	Fast using Fortran, supports openMP	Designed to work out-of-the-box with AVISO surface geostrophic velocities. Already configured to compute a broad range of Lagrangian diagnostics (i.e. Finite Time/Size Lyapunov Exponents; longitudinal and latitudinal origin of particles; time of particle retention within mesoscale eddies etc.)	Modular, fast, parallel; Multi-grid support; Used in a wide variety of contexts, from marine ecology to physical oceanography	Ease-of-use, customizable extension interface and automated performance optimization
Shortcomings	No parallel mode; trajectory scheme is somewhat crude beyond the context of 3D water mass tracing	Need of improving the diffusion	Non-scalable parallelization, not very efficient in reading large model output	Particle advection only 2D; cannot be run in parallel.	No support for non-orthogonal grids; parallel implementation is heavy on I/O	Not yet parallel; support for unstructured meshes in progress

Figure A.2: Continuation of the summary of the specifications of Lagrangian Particle Tracking tools from Van Sebille et al. (2018)

Code name	LIGHT in MPAS-O	NEMO online floats and icebergs	MITgcm	HYCOM Float Package	ROMS online floats
Website	mpas-dev.github.io	nemo-ocean.eu/About-NEMO/Reference-manuals	mitgcm.org	hycom.org	myroms.org/wiki/floats.in
License	Copyright (c) 2013, Los Alamos National Security, LLC (LANS) and the University Corporation for Atmospheric Research (UCAR).	CeCILL (http://www.cecill.info)	None	None	Open source MIT/X
Key citation	Wolfram et al. (2015)	Madec and NEMO team (2016) for floats; Marsh et al. (2015) for icebergs	Marshall et al. (1997a)	Halliwell and Garraffo (2002), Garraffo et al. (2001a); 2001b)	Piñones et al. (2011), Narvaez et al. (2012b)
OGCMs supported	Model for Prediction Across Scales Ocean (MPAS-O) (Ringler et al., 2013)	NEMO	MITgcm	Hybrid Coordinate Ocean Model (HYCOM) (Bleck, 2002; Chassignet et al., 2003; 2006)	ROMS
Language(s)	Fortran (post-processing in python)	Fortran	Fortran	Fortran	Fortran
Primary use	Large scale oceanography, diagnosing ocean mixing	Floats: large-scale, eddying ocean circulation. Icebergs: coupling of iceberg fluxes with ocean physics and dynamics and sea ice, via heat, freshwater and momentum fluxes; evaluating/ forecasting iceberg hazard	Ocean modelling at all scales, offline advection	Large scale and coastal oceanography, biology	Coastal and mesoscale oceanography, Individual Based modelling for biophysical applications
Advection method	Sub-stepped generalized RK for time integration; Wachspress and RBF horizontal interpolation; linear vertical and temporal interpolation	Floats: Ariane method or RK4. Icebergs: RK4	RK4	RK4	4th-order Milne predictor and 4th-order Hamming corrector
Diffusion method	None	None	Brownian motion optional	Brownian motion optional	Vertical random walk optional
Grids supported	Unstructured C-grid	Arakawa C	Arakawa C	Arakawa C	Arakawa C
Key strengths	Fast (minimal cost to OGCM), high temporal and spatial fidelity, computes isopycnal advection by construction, extensible within Fortran framework	Floats: Analytical advection on model timestep resolution. Icebergs: freshwater flux due to melting icebergs	Works well with archived MITgcm velocity fields, scales to very large sizes using MPI and domain tiling	Stable and relatively easy to use and understand	Reliable since trajectories are coherent with ocean circulation, parallel, easy to set up
Shortcomings	Currently no explicit offline mode, tied to MPAS framework and presently embedded in MPAS-O	Floats: limited use/publications to date. Icebergs: physics and dynamics subject to several uncertain parameters; giant tabular icebergs not yet represented; interactions with sea ice currently limited	Complicated to set up	No parallel mode	Computationally expensive since no offline model is available; Large output files for long runs or many particles.

Figure A.3: Some existing trajectory models for various oceanic and atmospheric applications from Dagestad et al. (2018).

Name	Reference/URL	Main application
Ariane	Blanke et al. (1997)	Oceanography
BSHDmod	Dick and Soetje (1990)	Oil
Connectivity Modeling System	Paris et al. (2013)	Ocean, generic
CIS iceberg model	Kubat et al. (2007)	Icebergs
CLaMS	McKenna et al. (2002)	Atmospheric chemistry
EMEP	Simpson et al. (2012)	Air pollution
FLEXPART, FLEXSTRA	www.flexpart.eu, Stohl et al. (1995)	Nuclear, air pollution
HYSPLIT	Stein et al. (2015)	Atmospheric transport
Ladim	Ådlandsvik and Sundby (1994)	Plankton transport
LAGRANTO	Wernli and Davies (1997), Sprenger and Wernli (2015)	Meteorology
LAGRANTO.ocean	Schemm et al. (2017)	Water mass properties
Leeway	Breivik and Allen (2008), Allen and Plourde (1999)	Search and rescue
LTRANS	Schlag and North (2012)	Plankton (including larvae)
MEDSLIK, MEDSLIK-II	De Dominicis et al. (2013), Lardner et al. (1998)	Oil
MIKE	www.mikepoweredbydhi.com	Ocean, generic
MOHID	www.mohid.com	Oil, sediments, water quality
MOTHY	Daniel (1996)	Oil, drifting objects
OD3D	Wettre et al. (2001)	Oil
OILMAP, SIMAP, CHEMMAP, MUDMAP, SARMAP	www.asascience.com	Oil, sediments, chemical, search and rescue
OILTOX	Brovchenko et al. (2003)	Oil
OILTRANS	Berry et al. (2012)	Oil
OSCAR	www.sintef.no/en/software/oscar	Oil
OSERIT	oserit.mumm.ac.be	Oil, chemicals
PARCELS	https://github.com/OceanPARCELS/parcels	Ocean, generic
POSEIDON-OSM	osm.hcmr.gr	Oil
PyGNOME/GNOME	gnome.orr.noaa.gov	Oil, generic
SeaTrackWeb, PADM	stw.smhi.se	Oil, chemicals
SNAP	Bartnicki et al. (2016)	Atmospheric nuclear transport
STILT	www.stilt-model.org	Atmospheric trace gases
THREETOX	Margvelashvily et al. (1997)	Nuclear ocean transport
TRACMASS	Döös et al. (2013)	Ocean and atmosphere, generic
VOS	en.ferhri.org	Oil

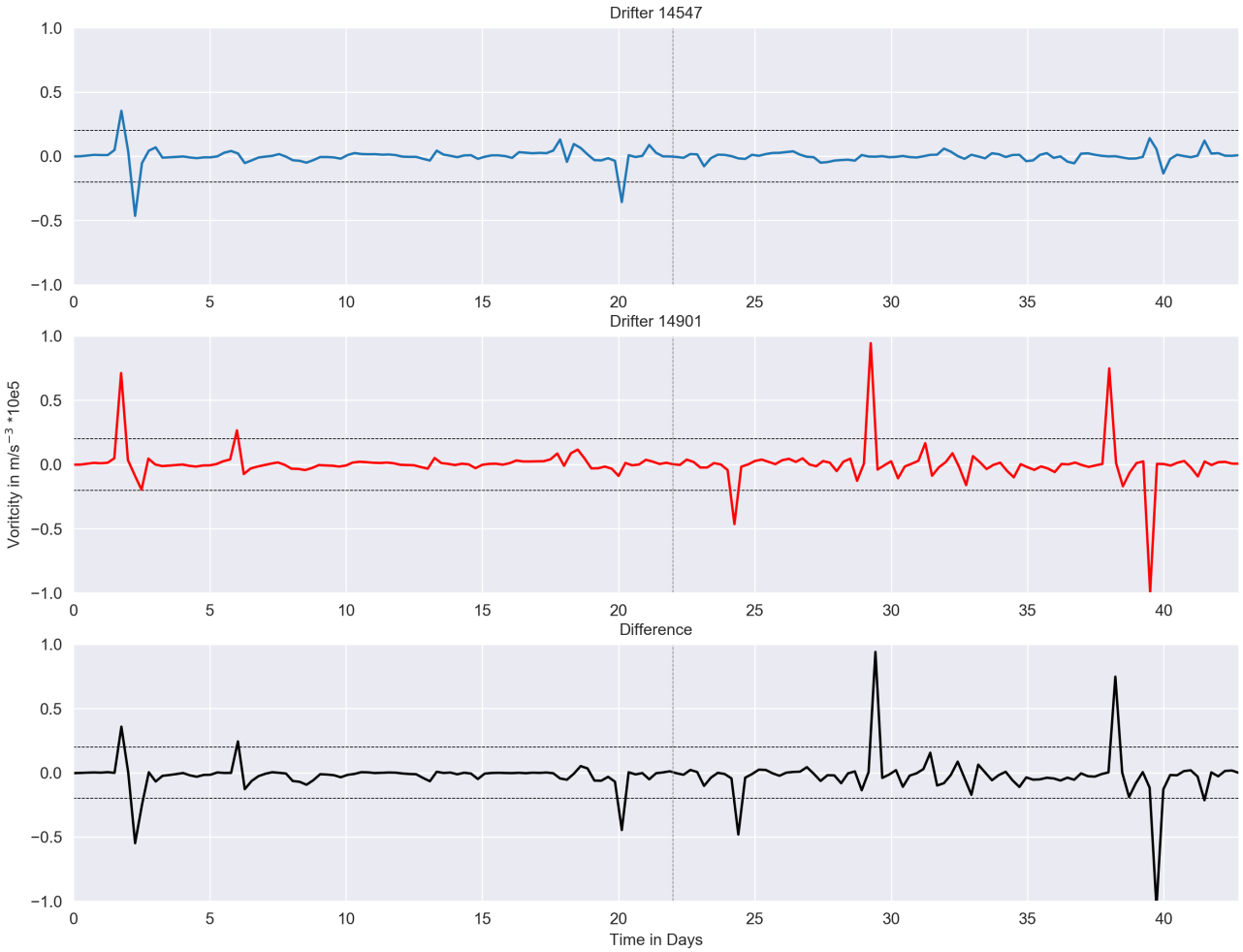

Figure A.4: Vorticity of the drifter 14547 (blue) and drifter 14901 (red) calculated throughout the drifter trajectories. A threshold of 0.00002 and - 0.00002 was chosen to find high values of vorticity that could result in divergence of the drifter trajectories.

References

Abernathey, R. P. and Marshall, J. (2013). Global surface eddy diffusivities derived from satellite altimetry. *Journal of Geophysical Research: Oceans*, 118(2):901–916.

Allen, A. A. and Plourde, J. V. (1999). Review of leeway: field experiments and implementation. Technical report, Coast Guard Research and Development Center Groton CT.

Atkinson, L. P. (2010). Western boundary currents. In *Carbon and nutrient fluxes in continental margins*, pages 121–169. Springer.

Awaji, T., Imasato, N., and Kunishi, H. (1980). Tidal exchange through a strait: A numerical experiment using a simple model basin. *Journal of Physical Oceanography*, 10(10):1499–1508.

Backeberg, B. and Reason, C. (2010). A connection between the South Equatorial Current north of Madagascar and Mozambique Channel eddies. *Geophysical Research Letters*, 37(4).

Backeberg, B. C., Counillon, F., Johannessen, J. A., and Pujol, M.-I. (2014). Assimilating along-track SLA data using the EnOI in an eddy resolving model of the Agulhas system. *Ocean Dynamics*, 64(8):1121–1136.

Backeberg, B. C., Johannessen, J. A., Bertino, L., and Reason, C. (2008). The greater Agulhas Current system: An integrated study of its mesoscale variability. *Journal of Operational Oceanography*, 1(1):29–44.

Bakhoday-Paskyabi, M. (2015). Particle motions beneath irrotational water waves. *Ocean Dynamics*, 65(8):1063–1078.

Bakhoday-Paskyabi, M. (2016). Turbulence-particle interactions under surface gravity waves. *Ocean Dynamics*, 66(11):1429–1448.

Barceló, C., Domingo, A., Miller, P., Ortega, L., Giffoni, B., Sales, G., McNaughton, L., Marcovaldi, M., Heppell, S. S., and Swimmer, Y. (2013). High-use areas, seasonal movements and dive patterns of juvenile loggerhead sea turtles in the Southwestern Atlantic Ocean. *Marine Ecology Progress Series*, 479:235–250.

Barron, C. N., Smedstad, L. F., Dastugue, J. M., and Smedstad, O. M. (2007). Evaluation of ocean models using observed and simulated drifter trajectories: Impact of sea surface height on synthetic profiles for data assimilation. *Journal of Geophysical Research: Oceans*, 112(C7).

Beal, L. M. and Bryden, H. L. (1997). Observations of an Agulhas undercurrent. *Deep Sea Research Part I: Oceanographic Research Papers*, 44(9-10):1715–1724.

Beal, L. M. and Bryden, H. L. (1999). The velocity and vorticity structure of the Agulhas Current at 32 S. *Journal of Geophysical Research: Oceans*, 104(C3):5151–5176.

Beal, L. M., De Ruijter, W. P., Biastoch, A., Zahn, R., Cronin, M., Hermes, J., Lutjeharms, J., Quartly, G., Tozuka, T., Baker-Yeboah, S., et al. (2011). On the role of the Agulhas system in ocean circulation and climate. *Nature*, 472(7344):429.

Beal, L. M., Elipot, S., Houk, A., and Leber, G. M. (2015). Capturing the transport variability of a western boundary jet: Results from the Agulhas Current Time-Series Experiment (ACT). *Journal of Physical Oceanography*, 45(5):1302–1324.

Biastoch, A., Böning, C. W., Getzlaff, J., Molines, J.-M., and Madec, G. (2008a). Causes of interannual–decadal variability in the meridional overturning circulation of the midlatitude North Atlantic Ocean. *Journal of Climate*, 21(24):6599–6615.

Biastoch, A., Böning, C. W., and Lutjeharms, J. (2008b). Agulhas leakage dynamics affects decadal variability in Atlantic overturning circulation. *Nature*, 456(7221):489.

Black, K., Athey, S., Wilson, P., and Evans, D. (2004). Particle Tracking: a new tool for coastal zone sediment management. In *Proceedings of the 4th International Conference, Littoral'04, Aberdeen, September*, pages 525–530.

Blanke, B., Penven, P., Roy, C., Chang, N., and Kokoszka, F. (2009). Ocean variability over the Agulhas Bank and its dynamical connection with the southern Benguela upwelling system. *Journal of Geophysical Research: Oceans*, 114(C12).

Bogucki, D. J., Jones, B. H., and Carr, M.-E. (2005). Remote measurements of horizontal eddy diffusivity. *Journal of Atmospheric and Oceanic Technology*, 22(9):1373–1380.

Bolten, A. B. (2003a). Active swimmers-passive drifters: the oceanic juvenile stage of loggerheads in the Atlantic system. *Loggerhead sea turtles*, pages 63–78.

Bolten, A. B. (2003b). Variation in sea turtle life history patterns: neritic vs. oceanic developmental stages. *The biology of sea turtles*, 2:243–257.

Braby, L., Backeberg, B. C., Ansorge, I., Roberts, M. J., Krug, M., and Reason, C. J. (2016). Observed eddy dissipation in the Agulhas Current. *Geophysical Research Letters*, 43(15):8143–8150.

Breivik, Ø. and Allen, A. A. (2008). An operational search and rescue model for the Norwegian Sea and the North Sea. *Journal of Marine Systems*, 69(1-2):99–113.

Breivik, Ø., Allen, A. A., Maisondieu, C., and Roth, J. C. (2011). Wind-induced drift of objects at sea: The leeway field method. *Applied Ocean Research*, 33(2):100–109.

Briscoe, D., Parker, D., Balazs, G., Kurita, M., Saito, T., Okamoto, H., Rice, M., Polovina, J., and Crowder, L. (2016). Active dispersal in loggerhead sea turtles (Caretta caretta) during the 'lost years'. *Proceedings of the Royal Society B: Biological Sciences*, 283(1832):20160690.

Cancet, M., Griffin, D., Cahill, M., Chapron, B., Johannessen, J., and Donlon, C. (2019). Evaluation of GlobCurrent surface ocean current products: A case study in Australia. *Remote sensing of environment*, 220:71–93.

Carlson, D. F., Fredj, E., Gildor, H., and Rom-Kedar, V. (2010). Deducing an upper bound to the horizontal eddy diffusivity using a stochastic Lagrangian model. *Environmental fluid mechanics*, 10(5):499–520.

Carr, A. (1986). Rips, FADS, and little loggerheads. *Bioscience*, 36(2):92–100.

Casal, T. G., Beal, L. M., Lumpkin, R., and Johns, W. E. (2009). Structure and downstream evolution of the agulhas current system during a quasi-synoptic survey in february–march 2003. *Journal of Geophysical Research: Oceans*, 114(C3).

Chao, Y., Li, Z., Farrara, J. D., and Hung, P. (2009). Blending sea surface temperatures from multiple satellites and in situ observations for coastal oceans. *Journal of atmospheric and oceanic technology*, 26(7):1415–1426.

Cheng, Y., Putrasahan, D., Beal, L., and Kirtman, B. (2016). Quantifying Agulhas leakage in a high-resolution climate model. *Journal of Climate*, 29(19):6881–6892.

Collins, C. and Hermes, J. (2019). Modelling the accumulation and transport of floating marine micro-plastics around South Africa. *Marine pollution bulletin*, 139:46–58.

Cushman-Roisin, B. and Beckers, J.-M. (2011). *Introduction to geophysical fluid dynamics: physical and numerical aspects*, volume 101. Academic press.

da Silveira, I. C., Flierl, G. R., and Brown, W. S. (1999). Dynamics of separating western boundary currents. *Journal of physical oceanography*, 29(2):119–144.

Dagestad, K.-F. and Röhrs, J. (2019). Prediction of ocean surface trajectories using satellite derived vs. modeled ocean currents. *Remote sensing of environment*, 223:130–142.

Dagestad, K.-F., Röhrs, J., Breivik, Ø., and Ådlandsvik, B. (2018). OpenDrift v1. 0: a generic framework for trajectory modelling. *Geoscientific Model Development*, 11(4):1405–1420.

Davis, R. E. (1991). Observing the general circulation with floats. *Deep Sea Research Part A. Oceanographic Research Papers*, 38:S531–S571.

de Ruijter, W. P., Van Leeuwen, P. J., and Lutjeharms, J. R. (1999). Generation and evolution of Natal Pulses: solitary meanders in the Agulhas Current. *Journal of physical oceanography*, 29(12):3043–3055.

Delandmeter, P. and van Sebille, E. (2019). The Parcels v2. 0 Lagrangian framework: new field interpolation schemes. *Geosci. Model Dev. Discuss.*

d'Hotman, J. S., Malan, N., Collins, C., de Vos, M., Lumpkin, R., Morris, T., and Hermes, J. (2019). The use of a jet reference frame to analyze drifter trajectories in the Agulhas Current. *Journal of Geophysical Research: Oceans*.

Doglioli, A., Veneziani, M., Blanke, B., Speich, S., and Griffa, A. (2006). A Lagrangian analysis of the Indian-Atlantic interocean exchange in a regional model. *Geophysical Research Letters*, 33(14).

Drivdal, M., Broström, G., and Christensen, K. (2014). Wave-induced mixing and transport of buoyant particles: application to the Statfjord A oil spill. *Ocean Science*, 10(6):977–991.

Duncan, E. M., Arrowsmith, J., Bain, C., Broderick, A. C., Lee, J., Metcalfe, K., Pikesley, S. K., Snape, R. T., van Sebille, E., and Godley, B. J. (2018). The true depth of the Mediterranean plastic problem: Extreme microplastic pollution on marine turtle nesting beaches in Cyprus. *Marine pollution bulletin*, 136:334–340.

Durgadoo, J. V., Loveday, B. R., Reason, C. J., Penven, P., and Biastoch, A. (2013). Agulhas leakage predominantly responds to the Southern Hemisphere westerlies. *Journal of Physical Oceanography*, 43(10):2113–2131.

Ekman, V. W. (1905). On the influence of the earth's rotation on ocean-currents. *Arkiv for Matematik, Astronomi Och Fysik*.

Freitas, C., Caldeira, R., and Dellinger, T. (2019). Surface behavior of pelagic juvenile loggerhead sea turtles in the eastern North Atlantic. *Journal of experimental marine biology and ecology*, 510:73–80.

Friedlander, S. (1980). *An introduction to the mathematical theory of geophysical fluid dynamics*, volume 41. Elsevier.

Garcia-Jove, M., Sheinbaum, J., and Jouanno, J. (2016). Sensitivity of Loop Current metrics and eddy detachments to different model configurations: The impact of topography and Caribbean perturbations. *Atmósfera*, 29(3):235–265.

Garzoli, S. L., Gordon, A. L., Kamenkovich, V., Pillsbury, D., and Duncombe-Rae, C. (1996). Variability and sources of the southeastern Atlantic circulation. *Journal of Marine Research*, 54(6):1039–1071.

Gonella, J. (1971). A local study of inertial oscillations in the upper layers of the ocean. In *Deep Sea Research and Oceanographic Abstracts*, volume 18, pages 775–788. Elsevier.

Gordon, A. L. (1986). Interocean exchange of thermocline water. *Journal of Geophysical Research: Oceans*, 91(C4):5037–5046.

Gründlingh, M. L. (1983). On the course of the Agulhas Current. *South African Geographical Journal*, 65(1):49–57.

Hart-Davis, M., Backeberg, B., and Bakhoday-Paskyabi (2018a). An assessment of the importance of combining wind, ocean currents and stochastic motions in a particle trajectory model for search and rescue applications. *South African Society For Atmospheric Sciences*, 34:157 – 160.

Hart-Davis, M. G., Backeberg, B. C., Halo, I., van Sebille, E., and Johannessen, J. A. (2018b). Assessing the accuracy of satellite derived ocean currents by comparing observed and virtual buoys in the Greater Agulhas Region. *Remote Sensing of Environment*, 216:735–746.

Hazen, E. L., Maxwell, S. M., Bailey, H., Bograd, S. J., Hamann, M., Gaspar, P., Godley, B. J., and Shillinger, G. L. (2012). Ontogeny in marine tagging and tracking science: technologies and data gaps. *Marine Ecology Progress Series*, 457:221–240.

Hida, T. (1980). Brownian motion. In *Brownian Motion*, pages 44–113. Springer.

Huang, N. E. (1979). On surface drift currents in the ocean. *Journal of Fluid Mechanics*, 91(1):191–208.

Imasato, N., Awaji, T., and Kunishi, H. (1980). Tidal exchange through naruto, akashi and kitan straits. *Journal of the Oceanographical Society of Japan*, 36(3):151–162.

Imawaki, S., Bower, A. S., Beal, L., and Qiu, B. (2013). Western boundary currents. In *International Geophysics*, volume 103, pages 305–338. Elsevier.

Imbol Nkwinkwa, N., Rouault, M., and Johannessen, J. A. (2019). Latent Heat Flux in the Agulhas Current. *Remote Sensing*, 11(13):1576.

Kelly, K. A. and Dong, S. (2004). The relationship of western boundary current heat transport and storage to midlatitude ocean-atmosphere interaction. *Earth's Climate: The Ocean–Atmosphere Interaction, Geophys. Monogr*, 147:347–363.

King, L., Weingartner, T., and Danielson, S. (2002). Nearshore Circulation in the Bering Sea: Towards Community-Based Oceanographic Research. *CFOS*.

Krug, M. and Tournadre, J. (2012). Satellite observations of an annual cycle in the Agulhas Current. *Geophysical Research Letters*, 39(15).

LaCasce, J. (2000). Floats and f/H. *Journal of Marine Research*, 58(1):61–95.

LaCasce, J. (2008). Statistics from Lagrangian observations. *Progress in Oceanography*, 77(1):1–29.

LaCasce, J., Ferrari, R., Marshall, J., Tulloch, R., Balwada, D., and Speer, K. (2014). Float-derived isopycnal diffusivities in the DIMES experiment. *Journal of Physical Oceanography*, 44(2):764–780.

Lacerda, A. L. d. F., Rodrigues, L. d. S., van Sebille, E., Rodrigues, F. L., Ribeiro, L., Secchi, E. R., Kessler, F., and Proietti, M. C. (2019). Plastics in sea surface waters around the Antarctic Peninsula. *Scientific reports*, 9(1):3977.

Lacorata, G., Corrado, R., Falcini, F., and Santoleri, R. (2019). FSLE analysis and validation of Lagrangian simulations based on satellite-derived GlobCurrent velocity data. *Remote sensing of environment*, 221:136–143.

Lange, M. and van Sebille, E. (2017). Parcels v0. 9: prototyping a Lagrangian ocean analysis framework for the petascale age. *arXiv preprint arXiv:1707.05163*.

Le Bars, D., Dijkstra, H., and De Ruijter, W. (2013). Impact of the Indonesian Throughflow on Agulhas leakage. *Ocean Science Discussions*, 10:353–391.

Lévêque, E., Toschi, F., Shao, L., and Bertoglio, J.-P. (2007). Shear-improved Smagorinsky model for large-eddy simulation of wall-bounded turbulent flows. *Journal of Fluid Mechanics*, 570:491–502.

Liu, Y., Weisberg, R. H., Hu, C., Kovach, C., and Riethmüller, R. (2011). Evolution of the Loop Current system during the Deepwater Horizon oil spill event as observed with drifters and satellites. *Monitoring and Modeling the Deepwater Horizon Oil Spill: A Record-Breaking Enterprise, Geophys. Monogr. Ser*, 195:91–101.

Lohmann, K. and Lohmann, C. (1996). Orientation and open-sea navigation in sea turtles. *Journal of Experimental Biology*, 199(1):73–81.

Lumpkin, R., Özgökmen, T., and Centurioni, L. (2017). Advances in the application of surface drifters. *Annual Review of Marine Science*, 9:59–81.

Lutjeharms, J. and Ansorge, I. (2001). The Agulhas Return Current. *Journal of Marine Systems*, 30(1-2):115–138.

Lutjeharms, J., Boebel, O., and Rossby, H. (2003). Agulhas cyclones. *Deep Sea Research Part II: Topical Studies in Oceanography*, 50(1):13–34.

Lutjeharms, J. and Roberts, H. (1988). The Natal pulse: An extreme transient on the Agulhas Current. *Journal of Geophysical Research: Oceans*, 93(C1):631–645.

Lutjeharms, J. and Valentine, H. (1988). Eddies at the subtropical convergence south of Africa. *Journal of Physical Oceanography*, 18(5):761–774.

Lutjeharms, J. and Van Ballegooyen, R. (1988). The Retroflection of the Agulhas Current. *Journal of Physical Oceanography*, 18(11):1570–1583.

Lutjeharms, J. R. (2006). *The Agulhas Current*, volume 2. Springer.

Machado, A. and Bermejo, J. (2012). Estado de conservación de la tortuga boba (Caretta caretta) en las islas Canarias. *Plan de seguimiento de la tortuga boba en Canarias. Santa Cruz de Tenerife: Observatorio Ambiental Granadilla*.

MarineBio (2019). Loggerhead Turtles. *MarineBio*.

McAdam, R. and van Sebille, E. (2018). Surface Connectivity and Interocean Exchanges From Drifter-Based Transition Matrices. *Journal of Geophysical Research: Oceans*, 123(1):514–532.

McInnes, A. S., Laczka, O. F., Baker, K. G., Larsson, M. E., Robinson, C. M., Clark, J. S., Laiolo, L., Alvarez, M., Laverock, B., Kremer, C. T., et al. (2019). Live cell analysis at sea reveals divergent thermal performance between photosynthetic ocean microbial eukaryote populations. *The ISME journal*, page 1.

Morris, T., Brummer, G.-J., and Louw, G. (2015). Cruise Report Agulhas System Climate Array (ASCA) Cruise. *SAEON*, pages 1–73.

Morris, T., Hermes, J., Beal, L., Du Plessis, M., Rae, C. D., Gulekana, M., Lamont, T., Speich, S., Roberts, M., and Ansorge, I. J. (2017). The importance of monitoring the Greater Agulhas Current and its inter-ocean exchanges using large mooring arrays. *South African Journal of Science*, 113(7-8):1–7.

Nel, R., Punt, A. E., and Hughes, G. R. (2013). Are coastal protected areas always effective in achieving population recovery for nesting sea turtles? *PloS one*, 8(5):e63525.

Nkwinkwa Njouodo, A. S., Koseki, S., Keenlyside, N., and Rouault, M. (2018). Atmospheric signature of the Agulhas Current. *Geophysical Research Letters*, 45(10):5185–5193.

NOAA (2019). Global Drifter Program . *NOAA*.

NSRI (2018). Key Rescue Statistic from 2017. *NSRI*.

Ocean, J. O. (2010). GHRSST Level 4 G1SST Global Foundation Sea Surface Temperature Analysis; JPL OurOcean Project; NASA PO. *DAAC: Pasadena, CA, USA*.

Oh, I. S., Zhurbas, V., and Park, W. (2000). Estimating horizontal diffusivity in the East Sea (Sea of Japan) and the northwest Pacific from satellite-tracked drifter data. *Journal of Geophysical Research: Oceans*, 105(C3):6483–6492.

Olson, D. B. and Evans, R. H. (1986). Rings of the Agulhas Current. *Deep Sea Research Part A. Oceanographic Research Papers*, 33(1):27–42.

Onink, V. (2018). Modeling the accumulation of floating microplastic in the subtropical ocean gyres. Master's thesis, University of Utrecht.

Onink, V., Wichmann, D., Delandmeter, P., and Van Sebille, E. (2018). The role of Ekman currents, geostrophy and Stokes drift in the accumulation of floating microplastic. *Journal of Geophysical Research: Oceans*.

Parsiegla, N., Gohl, K., and Uenzelmann-Neben, G. (2008). The Agulhas Plateau: Structure and evolution of a large igneous province. *Geophysical Journal International*, 174(1):336–350.

Pichevin, T., Nof, D., and Lutjeharms, J. (1999). Why are there Agulhas rings? *Journal of physical oceanography*, 29(4):693–707.

Pollard, R. (1980). Properties of near-surface inertial oscillations. *Journal of Physical Oceanography*, 10:385–398.

Pollard, R. T. and Millard Jr, R. (1970). Comparison between observed and simulated wind-generated inertial oscillations. In *Deep Sea Research and Oceanographic Abstracts*, volume 17, pages 813–821. Elsevier.

Poulain, P.-M. and Centurioni, L. (2015). Direct measurements of World Ocean tidal currents with surface drifters. *Journal of Geophysical Research: Oceans*, 120(10):6986–7003.

Ragoasha, N., Herbette, S., Cambon, G., Veitch, J., Reason, C., and Roy, C. (2019). Lagrangian pathways in the southern Benguela upwelling system. *Journal of Marine Systems*, 195:50–66.

Renault, L., McWilliams, J. C., and Penven, P. (2017). Modulation of the Agulhas Current Retroflection and leakage by oceanic current interaction with the atmosphere in coupled simulations. *Journal of Physical Oceanography*, 47(8):2077–2100.

Reynolds, R. W., Zhang, H.-M., Smith, T. M., Gentemann, C. L., and Wentz, F. (2005). Impacts of in situ and additional satellite data on the accuracy of a sea-surface temperature analysis for climate. *International Journal of Climatology: A Journal of the Royal Meteorological Society*, 25(7):857–864.

Rio, M., Mulet, S., and Picot, N. (2013). New global Mean Dynamic Topography from a GOCE geoid model, altimeter measurements and oceanographic in-situ data. In *Proceedings of the ESA living planet symposium, Edinburgh*.

Rio, M.-H., Mulet, S., and Picot, N. (2014). Beyond GOCE for the ocean circulation estimate: Synergetic use of altimetry, gravimetry, and in situ data provides new insight into geostrophic and Ekman currents. *Geophysical Research Letters*, 41(24):8918–8925.

Rouault, M. J., Mouche, A., Collard, F., Johannessen, J., and Chapron, B. (2010). Mapping the Agulhas Current from space: An assessment of ASAR surface current velocities. *Journal of Geophysical Research: Oceans*, 115(C10).

Rühs, S., Zhurbas, V., Koszalka, I. M., Durgadoo, J. V., and Biastoch, A. (2018). Eddy Diffusivity Estimates from Lagrangian Trajectories Simulated with Ocean Models and Surface Drifter Data—A Case Study for the Greater Agulhas System. *Journal of Physical Oceanography*, 48(1):175–196.

Sayol, J. M., Orfila, A., Simarro, G., Conti, D., Renault, L., and Molcard, A. (2014). A Lagrangian model for tracking surface spills and SaR operations in the ocean. *Environmental modelling & software*, 52:74–82.

Schwarzkopf, F. U., Biastoch, A., Böning, C. W., Chanut, J., Durgadoo, J. V., Getzlaff, K., Harlaß, J., Rieck, J. K., Roth, C., Scheinert, M. M., and Schubert, R. (2019). The INALT family–a set of high-resolution nests for the Agulhas Current system within global NEMO ocean/sea-ice configurations. *Geoscientific Model Development Discussions*, pages 1–44.

Scott, R., Biastoch, A., Agamboue, P. D., Bayer, T., Boussamba, F. L., Formia, A., Godley, B. J., Mabert, B. D. K., Manfoumbi, J. C., Schwarzkopf, F. U., Sounguet, G.-P., Wagner, P., and Witt, M. J. (2017). Spatio-temporal variation in ocean current-driven hatchling dispersion: Implications for the world's largest leatherback sea turtle nesting region. *Diversity and Distributions*, 23(6):604–614.

Seager, R. and Simpson, I. R. (2016). Western boundary currents and climate change. *Journal of Geophysical Research: Oceans*, 121(9):7212–7214.

Shamblin, B. M., Bolten, A. B., Abreu-Grobois, F. A., Bjorndal, K. A., Cardona, L., Carreras, C., Clusa, M., Monzón-Argüello, C., Nairn, C. J., Nielsen, J. T., et al. (2014). Geographic patterns of genetic variation in

a broadly distributed marine vertebrate: new insights into loggerhead turtle stock structure from expanded mitochondrial DNA sequences. *PLoS One*, 9(1):e85956.

Singh, S. P., Groeneveld, J. C., Hart-Davis, M. G., Backeberg, B. C., and Willows-Munro, S. (2018). Seascape genetics of the spiny lobster Panulirus homarus in the Western Indian Ocean: Understanding how oceanographic features shape the genetic structure of species with high larval dispersal potential. *Ecology and Evolution*, 8(23):12221–12237.

Smagorinsky, J. (1963). General circulation experiments with the primitive equations: I. The basic experiment. *Monthly weather review*, 91(3):99–164.

Soulsby, R., Mead, C., and Wild, B. (2007). A model for simulating the dispersal tracks of sand grains in coastal areas:'SandTrack'. *Geological Society, London, Special Publications*, 274(1):65–72.

Strickland, R. (2006). Oceanography 101, Lecture 14. *University of Washington*.

Swenson, M. S. and Niiler, P. P. (1996). Statistical analysis of the surface circulation of the California Current. *Journal of Geophysical Research: Oceans*, 101(C10):22631–22645.

Takahashi, T., Sutherland, S. C., Wanninkhof, R., Sweeney, C., Feely, R. A., Chipman, D. W., Hales, B., Friederich, G., Chavez, F., Sabine, C., et al. (2009). Climatological mean and decadal change in surface ocean pCO2, and net sea–air CO2 flux over the global oceans. *Deep Sea Research Part II: Topical Studies in Oceanography*, 56(8-10):554–577.

Talley, L. D. (2011). *Descriptive physical oceanography: an introduction*. Academic press.

Taylor, G. I. (1922). Diffusion by continuous movements. *Proceedings of the london mathematical society*, 2(1):196–212.

Thorpe, S. E., Heywood, K. J., Stevens, D. P., and Brandon, M. A. (2004). Tracking passive drifters in a high resolution ocean model: implications for interannual variability of larval krill transport to South Georgia. *Deep Sea Research Part I: Oceanographic Research Papers*, 51(7):909–920.

Trotta, F., Pinardi, N., Fenu, E., Grandi, A., and Lyubartsev, V. (2017). Multi-nest high-resolution model of submesoscale circulation features in the Gulf of Taranto. *Ocean Dynamics*, 67(12):1609–1625.

Van den Bremer, T. and Breivik, Ø. (2017). Stokes drift. *Philosophical Transactions of the Royal Society A: Mathematical, Physical and Engineering Sciences*, 376(2111):20170104.

Van Sebille, E., Griffies, S. M., Abernathey, R., Adams, T. P., Berloff, P., Biastoch, A., Blanke, B., Chassignet, E. P., Cheng, Y., Cotter, C. J., et al. (2018). Lagrangian ocean analysis: Fundamentals and practices. *Ocean Modelling*, 121:49–75.

van Sebille, E., van Leeuwen, P. J., Biastoch, A., Barron, C., and De Ruijter, W. (2009). Lagrangian validation of numerical drifter trajectories using drifting buoys: Application to the Agulhas system. *Ocean Modelling*, 29(4):269–276.

van Sebille, E., Van Leeuwen, P. J., Biastoch, A., and de Ruijter, W. P. (2010). Flux comparison of Eulerian and Lagrangian estimates of Agulhas leakage: A case study using a numerical model. *Deep Sea Research Part I: Oceanographic Research Papers*, 57(3):319–327.

Veitch, J., Hermes, J., Lamont, T., Penven, P., and Dufois, F. (2018). Shelf-edge jet currents in the southern Benguela: A modelling approach. *Journal of Marine Systems*, 188:27–38.

Veitch, J. A. and Penven, P. (2017). The role of the Agulhas in the Benguela Current system: A numerical modeling approach. *Journal of Geophysical Research: Oceans*, 122(4):3375–3393.

Visser, A. W. (1997). Using random walk models to simulate the vertical distribution of particles in a turbulent water column. *Marine Ecology Progress Series*, 158:275–281.

Wakker, K., Zandbergen, R., Naeije, M., and Ambrosius, B. (1990). Geosat altimeter data analysis for the oceans around South Africa. *Journal of Geophysical Research: Oceans*, 95(C3):2991–3006.

Weitbrecht, V., Uijttewaal, W., and Jirka, G. H. (2004). 2-D particle tracking to determine transport characteristics in rivers with dead zones. *Shallow flows*, pages 477–484.

Wikipedia (2019). Geostrophic Currents. *Wikipedia*.

Zhurbas, V., Lyzhkov, D., and Kuzmina, N. (2014). Drifter-derived estimates of lateral eddy diffusivity in the World Ocean with emphasis on the Indian Ocean and problems of parameterisation. *Deep Sea Research Part I: Oceanographic Research Papers*, 83:1–11.